



**HAL**  
open science

# Liquid jet breakup in gaseous crossflow injected through a large diameter nozzle

Clément Rouaix, Alexei Stoukov, Yannick Bury, David Joubert, Dominique Legendre

► **To cite this version:**

Clément Rouaix, Alexei Stoukov, Yannick Bury, David Joubert, Dominique Legendre. Liquid jet breakup in gaseous crossflow injected through a large diameter nozzle. *International Journal of Multiphase Flow*, 2023, 163, pp.104419. 10.1016/j.ijmultiphaseflow.2023.104419 . hal-04098260

**HAL Id: hal-04098260**

**<https://hal.science/hal-04098260v1>**

Submitted on 15 May 2023

**HAL** is a multi-disciplinary open access archive for the deposit and dissemination of scientific research documents, whether they are published or not. The documents may come from teaching and research institutions in France or abroad, or from public or private research centers.

L'archive ouverte pluridisciplinaire **HAL**, est destinée au dépôt et à la diffusion de documents scientifiques de niveau recherche, publiés ou non, émanant des établissements d'enseignement et de recherche français ou étrangers, des laboratoires publics ou privés.

# Liquid jet breakup in gaseous crossflow injected through a large diameter nozzle

Clément Rouaix<sup>a</sup>, Alexei Stoukov<sup>a</sup>, Yannick Bury<sup>b</sup>, David Joubert<sup>c</sup>, Dominique Legendre<sup>a,\*</sup>

<sup>a</sup> Institut de Mécanique des Fluides de Toulouse (IMFT) - Université de Toulouse, CNRS-INPT-UPS, 31400 Toulouse, France

<sup>b</sup> Université de Toulouse, ISAE-Supaéro, 31055 Toulouse, France

<sup>c</sup> Keppclair Evolution, 231 rue Saint Honoré, 75001 Paris, France

## A B S T R A C T

### Keywords:

Liquid jet in gaseous crossflow

Large diameter

VOF volume of fluid simulation

Column breakup

Column penetration and expansion

Airtanker

Near nozzle field behavior of round liquid jets injected through large injector diameter (ranging from 0.2 to 0.6 m) into subsonic uniform gaseous crossflows is numerically investigated using the Volume of Fluid (VoF) method. The liquid jet to gas momentum ratio is ranging from 4.3 to 39 with a gas Weber number ranging from  $1.6 \times 10^4$  to  $5.3 \times 10^4$ . The large scale liquid water column main properties, such as primary breakup process, liquid column penetration height, liquid column expansion and column breakup point location are studied. Effects of several parameters on the liquid column evolution are investigated, namely the diameter injector, the liquid jet injection velocity and the gaseous crossflow velocity. It has been found that the surface breakup and column breakup mechanisms are both contributing to the liquid column fragmentation. The fragmentation at large scale is characterized by the generation of a significant number of well developed arm and leg structures that align with the airflow on the side and at the bottom of the liquid column. Correlations for the main liquid jet properties are proposed and compared with results previously obtained for smaller size liquid jet. Liquid column penetration height, width and column breakup height follow the same type of power laws that those observed for liquid jet at smaller size. The liquid jet evolution is compared to the water jet generated by the B747 airliner.

## 1. Introduction

Liquid Jet in Gaseous Crossflow (LJGC) have been developed for many different industrial and environmental applications, as for example in agricultural sprays, rocket engines, combustion application, cooling systems and liquid jet printer. These studies have considered injector of millimeter size or smaller. Wu et al. (1997a,b) performed experimental and theoretical studies using liquid jet of different liquids (pure water, water–alcohol, and water–glycerol mixtures). As reported, the primary breakup regime can be classified using the momentum ratio  $q$  and the gaseous Weber number  $We_g$ . The primary breakup of the liquid jet is usually divided into two main breakup modes, the column breakup (or bulk breakup) (CBU) and the surface (or shear) breakup (SBU) (Wu et al. 1997a, Mazallon et al. 1999, Madabhushi et al. 2006). CBU refers to liquid column pinched-off and liquid column rupture occurring at the column breakup position. It produces relatively large liquid fragments and droplet-like shape. SBU refers to liquid mass shedding and detached liquid structures stripped-off, taking place all along the liquid column trajectory, from the injector point to the CBU locations. It also produces isolated structure ligaments and droplets-like

shape, but relatively smaller than those arising from CBU. Other terms, can be found in literature to describe primary breakup modes, such as column fracture, arcade type breakup or bag-like breakup (Vich and Ledoux 1997). Both CBU and SBU always occur in LJGC atomization, with the possible prevail of one mode depending on the relative values of  $We_g$  and  $q$  (Mazallon et al., 1999; Madabhushi et al., 2006). CBU is in turn subdivided into different sub-regimes (Wu et al. 1997a, Sallam et al. 2004), such as among others : capillary/column breakup, (single) bag breakup, multimode breakup, shear breakup. Under some conditions, when the injection diameter  $d_j$  gets close or larger than the liquid capillary length, other primary CBU regime can appear, namely the multimode bag breakup (Scharfman et al. 2013).

LJGC have been widely investigated, both experimentally and numerically, revealing challenging issues to overcome. Experimental studies are facing accuracy problems according to the measurement technique employed, the complex operating conditions involved, and limitation in observing and capturing dense fog liquid spray in the near injector nozzle region (Broumand and Birouk 2016). Direct numerical approaches based on interface capturing methods, such as Level Set

\* Corresponding author.

E-mail address: [legendre@imft.fr](mailto:legendre@imft.fr) (D. Legendre).

(LS) (Pai et al. 2010, Herrmann et al. 2010, Behzad et al. 2012, 2016), Volume of Fluid (VoF) (Li and Soteriou 2016, 2018, Prakash et al. 2019) or CLSVOF (Mukundan et al. 2021) methods, have to manage severe numerical challenges, especially because of large liquid to jet density ratio  $\rho^*$  and viscosity ratio  $\mu^*$ , together with high shear stress at sharp moving and deforming interfaces. LJGC studies, whether experimental or numerical, are made complex because of the flow field complexity by itself, involving unsteady interface deformation and rupture. The large range of both time and length scales requests high temporal and spatial resolutions in order to correctly describe atomization process, making challenging and expensive the development of both direct numerical simulations and experimental methods.

The outstanding diversity of geometrical and physical parameters in LJGC is another well-known aspect responsible for the discrepancy between empirical relations deduced from experiment. Indeed, the problem has several parameters to consider with some of them difficult to control in experiments. Liquid jet may exhibit different level of turbulence intensity (Wu et al. 1995, Sallam et al. 2006) making the main atomization features even harder to apprehend. Some studies have investigated different liquid allowing to vary liquid properties such as density (Herrmann 2011), viscosity ratios (Li et al. 2017) and rheology (newtonian and non-newtonian). Additional parameters related to the upcoming airstream flow have been investigated such as high airstream pressure and/or temperature environment (Amighi et al. 2009, Lubarsky et al. 2012b, Amighi and Ashgriz 2019b,a, Liu et al. 2021), subsonic (Wu et al. 1997a) or supersonic (Yates 1971, Schetz et al. 1980), uniform (Lee et al. 2007) or non-uniform (Ryan 2006), swirled (Tambe and Jeng 2008), with shear layers (Tambe et al. 2007) or turbulent (Broumand et al. 2019). Some studies are considering injector nozzle shape and aspect ratio (Haven and Kurosaka 1997), nozzle internal flow (Ahn et al. 2006, Osta and Sallam 2010) or even liquid jet injection angle (Fuller et al. 1997, Costa et al. 2006). The effects of gaseous wall turbulence on liquid jet atomization have also been investigated, as well as nozzle locations by means of parameters enabling to control airstream boundary layer development (Chelko 1950, Yu et al. 2006, Kim et al. 2012).

As a consequence, it results in a huge number of literature on the subject, however mostly focusing on nozzle injector diameters of the order of a few millimeters or less. Interaction between an air cross flow and larger liquid column diameters, typically more than ten centimeters, have been significantly less investigated up to now, despite their importance for different kind of natural or engineering applications such as, for instance, hydraulic dams waterfalls, fire hoses or airtankers dropping systems for aerial firefighting. In order to overcome this lack of information for such large nozzle diameter, this numerical study aims at providing new results and understanding of the liquid column penetration, expansion and fragmentation at such large scales, considering injector diameter  $d_j$  ranging from 0.2 to 0.6 m.

In such a context, a numerical study is proposed here to decipher the dynamics of the large scale liquid jet breakup, atomization and dispersion, as well as quantitative information on the liquid column penetration, expansion and Column Breakup (CBU) location. Section 2 defines the problem under consideration, the range of parameter considered and propose a literature review with a main focus on the liquid column penetration and expansion. The numerical method and the tests performed to discuss the grid convergence as well as the turbulence model used for this study are presented in Section 3. The results are reported in Section 4 with the description of the physical mechanisms involved in the liquid column atomization at large scale as well as with the description of the liquid column penetration, its transverse expansion and the location of the column breakup.

## 2. Problem statement and literature review

### 2.1. General description of the flow field, state of the art

We consider a water liquid jet of density  $\rho_j$  and dynamic viscosity  $\mu_j$  injected throughout a circular orifice of diameter  $d_j$  along the vertical

downward direction  $-\vec{e}_y$  into a subsonic air crossflow moving along the horizontal direction  $\vec{e}_x$  as shown in Fig. 1.  $\rho_g$  and  $\mu_g$  are the air density and dynamic viscosity, respectively.  $\vec{e}_z$  is then the spanwise horizontal direction. The liquid is injected with a uniform velocity  $v_j$  and the air velocity is imposed uniform at the distance  $l$  from the orifice center. Gravity  $\vec{g} = -g\vec{e}_y$  is oriented according to the vertical direction, and capillary effects are taken into account through a constant surface tension  $\sigma$ .

According to the  $\Pi$  or Vashy-Buckingham theorem, this problem is fully described by five independent non-dimension numbers. From the literature of LJGC for smaller diameter, two main non dimensional numbers have been identified: the momentum flux ratio  $q$  that compares gas inertia to liquid inertia

$$q = \frac{\rho_j v_j^2}{\rho_g u_g^2} \quad (1)$$

and the gas Weber number  $We_g$  that compares gas inertia to capillary effect

$$We_g = \frac{\rho_g u_g^2 d_j}{\sigma} \quad (2)$$

Additional non dimensional numbers can be introduced such as the liquid jet Weber number  $We_j = \rho_j v_j^2 d_j / \sigma$ , the gas Reynolds number  $Re_g = \rho_g u_g d_j / \mu_g$ , the liquid jet Reynolds number  $Re_j = \rho_j v_j d_j / \mu_j$ , the liquid Ohnesorge number  $Oh_j = \mu_j / \sqrt{\sigma \rho_j d_j}$ , the liquid Bond number  $Bo = \rho_j g d_j^2 / \sigma$ , the density ratio  $\rho^* = \rho_j / \rho_g$  and the viscosity ratio  $\mu^* = \mu_j / \mu_g$ , the normalized distance of injection  $l/d_j$ . In all the configurations studied here, the flow is characterized by a relatively low Mach number ( $Ma < 0.27$ ) allowing to neglect gas compressibility effects.

The liquid jet penetration, spreading and expansion into the gaseous crossflow is usually described using the liquid jet vertical penetration  $y$ , sometimes called liquid jet trajectory, and the liquid jet lateral spread or expansion width  $z$ . The liquid CBU point where the column breaks is defined by its streamwise distance to the injector  $x_{BU}$  and its vertical penetration  $y_{BU}$  (see Fig. 1). A significant number of empirical correlations have been provided in literature in order to characterize  $y$ ,  $z$ ,  $x_{BU}$  and  $y_{BU}$ . A detailed review of these correlations can be found in Stenzler et al. (2006), Mashayek et al. (2008), Mashayek and Ashgriz (2011), No (2015), Broumand and Birouk (2016). They are also summarized in Table 1. Throughout the literature, the liquid jet trajectory  $y/d_j$  is usually reported as a function of  $q$ , and the normalized distance  $x/d_j$ . Other parameters can also be taken into account in the correlation of the trajectories, such as: viscosity ratio, temperature, pressure, density ratio, Reynolds and Weber numbers of the crossflow, etc. Existing correlations can be classified into three functional forms: power law, logarithmic law and exponential law.

As pointed out by Lubarsky et al. (2012a), the numerous correlations do not match and a unified correlation still needs to be proposed. Indeed, the impressive amount of correlations, especially for the liquid jet trajectory  $y/d_j$  results in significant quantitative discrepancies between each others due to several reasons. First, the outstanding number of experimental studies available in literature are based on different definition and methods. Indeed,  $y/d_j$  has been measured according to different criteria such as for instance using transverse jet extremities (Chelko, 1950; Hussein et al., 1982), location of maximum flux concentration (Smith and Mungal, 1998; Han et al., 2000), mean streamline locations in the center plane  $z/d_j = 0$  (Yuan and Street, 1998; Hussein et al., 1982), streamline based only on the upwind or downwind liquid column side, or even location of maximum velocities (Yuan and Street, 1998). Measurement can be conducted only on the liquid column or on the overall liquid jet flow field including the spray. Thus, different names have been employed like for instance the ‘‘liquid jet trajectory’’ which may refer to the liquid column trajectory between the injector nozzle and the CBU location, or the ‘‘liquid jet penetration’’ which may be associated to the maximal transverse height

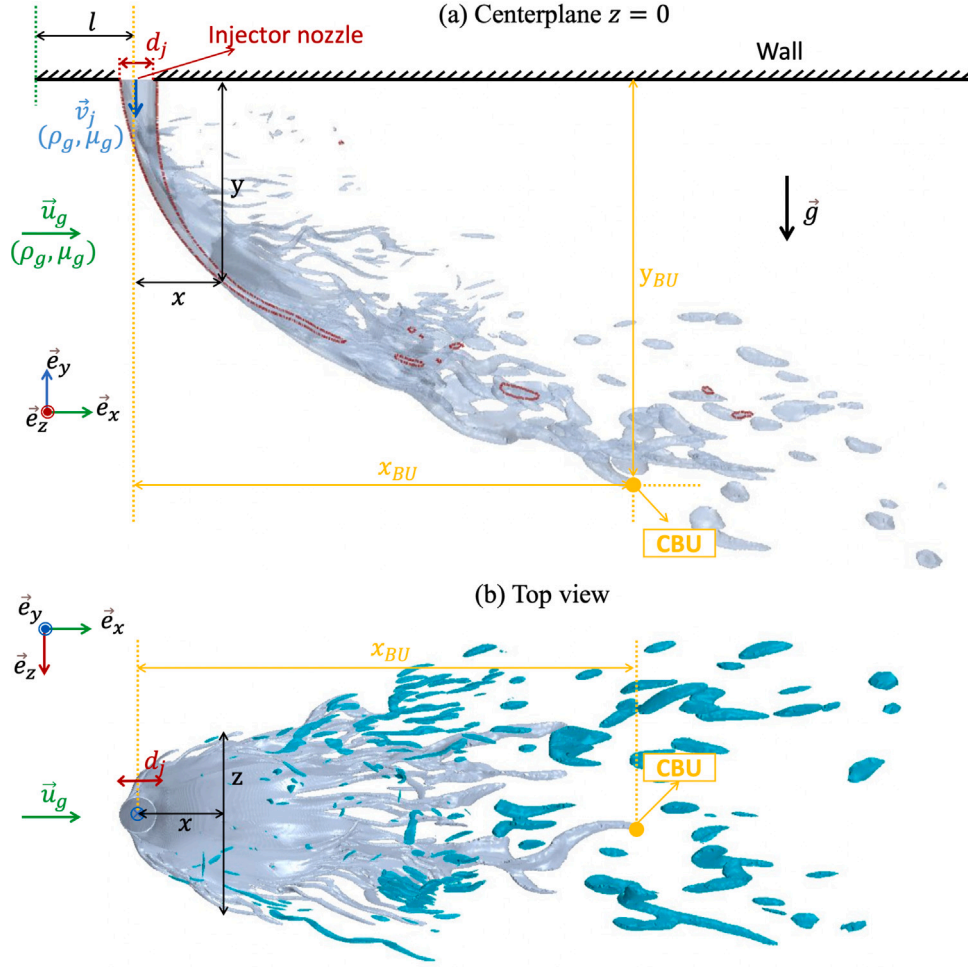


Fig. 1. Problem and variable definition based on a simulation at  $t = 4.5$  s for the reference case *Case1* for  $q = 17.3$  and  $We_g = 3.2 \times 10^4$  (see Table 3 for more details). (a) Side view and (b) top view.

or depth reached by the spray. Then, empirical correlations also depend on the flow field regions in which they are assessed, namely the near injector nozzle field (Wu et al., 1997a) or the so-called liquid jet far field (Yates, 1971). While exponential forms (Chen et al., 1993) allow to take into account three different regions of the liquid jet development and have proven to be reliable in the so-called far stream region, logarithmic laws generally provide better results in the near injector nozzle field (Gopala, 2012). Furthermore, measurement techniques employed, such as for example Particle Image Velocimetry (PIV), Mie scattering of light sheets (Cavaliere et al., 2003; Han et al., 2000), Phase Doppler Particle Analyser (PDPA) (Lin et al., 2002a), pulsed shadowgraphy (Mazallon et al., 1999), turn out to have a significant impact on LJGC flow field description. Indeed, some studies implementing PDPA highlighted that  $y/d_j$  prediction leads systematically to an over-estimation in comparison to shadowgraphy methods even when using strictly identical facility and experiment layout (Yates, 1971; Thomas and Schetz, 1985; Inamura et al., 1991; Lin et al., 2002a). Other reasons for such discrepancies on empirical correlations rely on the gaseous crossflow characteristics such as its turbulence level and possible non-uniformity together with the wall boundary layer development (Chelko, 1950; Cortelezzi and Karagozian, 2001). Gas crossflow entrainment by liquid jet far from the nozzle injector point may also have an impact on jet trajectory determination (Yuan and Street, 1998). Those correlations also depend on the range of parameters in which they have been consistently validated as well as some differences in operating conditions such as temperature and pressure having an impact in the density  $\rho^*$  and viscosity  $\mu^*$  ratios, ...), configuration layouts (single

or multiple injectors arranged in tandem or in square with flush or protruding tubes), liquid jet injection angle  $\theta_j$ , internal liquid flow pipe geometry (sharp or plain orifice with different nozzle aspect ratio) and consequently liquid jet turbulence level  $I_j$ .

## 2.2. Range of parameters

In this study, the velocity of both the liquid and the air as well as the injector diameter are varied in a range relevant when considering applications such as liquid ejection from a Large (LAT) to Very Large (VLAT) airtanker. For Aerial Fire Fighting purpose, aircrafts release liquid at velocity ranging from 50 to 70 m/s depending on the aircraft, and the liquid exit velocity can vary from 1 to 14 m/s. Considering the dropping system of the B747 made of 4 circular exits of 40 cm, the ground velocity can vary between 55 to 70 m/s and the liquid exit velocity can vary from 6 to 14 m/s. As a consequence, the selected values for  $v_j$ ,  $u_g$  and  $d_j$  are varied in the ranges [5 – 10] m/s, [50 – 90] m/s and [0.2 – 0.6] m, respectively. Table 2 reports the considered range of parameter and the corresponding non dimensional numbers. Table 3 gives the parameters used for the different simulations. Case 1 is considered as the reference case as it stands very close to the operating conditions of large and very large airtanker (LAT and VLAT). Cases 2 to 4 are used to study the grid convergence (see Section 3.3). Cases 5 to 7 are conducted to discuss the effect of the jet turbulence and its modeling (see Section 3.4). Cases 8 and 9 are performed to show the effect of the injector diameter  $d_j$ . Cases 10 to 12 are selected for the effect of the liquid injection velocity and Cases 13 and 14 for the velocity of the air crossflow.

**Table 1**

Table summarizing expressions from literature for liquid column penetration height  $y/d_j$ , expansion width  $z/d_j$ , and CBU location with streamwise length  $x_{BU}/d_j$  and height  $y_{BU}/d_j$ , showing different functional form with constant parameters  $\kappa$ ,  $\psi$ ,  $\xi$ ,  $\alpha$ ,  $\beta$ ,  $\gamma$ ,  $\theta$  and  $\delta$ .

	Parameters	Functional expression	References
$\frac{y}{d_j}$	$q$	$\frac{y}{d_j} = \kappa q^\alpha \left(\frac{x}{d_j}\right)^\beta$ (1.1)	Wu et al. (1997a) Birouk et al. (2007)
	$q, We_g$	$\frac{y}{d_j} = \kappa q^\alpha \left(\frac{x}{d_j}\right)^\beta We_g^\eta Z_1^\varphi Z_2^\theta$ (1.2)	Stenzler et al. (2003) Farvardin et al. (2013)
	$q$ , other	$\frac{y}{d_j} = \kappa q^\alpha \left(\frac{x}{d_j}\right)^\beta Z_1^\eta Z_2^\varphi$ (1.3)	Amighi et al. (2009) Eslamian et al. (2014)
	$q$	$\frac{y}{d_j} = \kappa q^\alpha \ln \left[ 1 + \left( \beta \frac{x}{d_j} \right) \right]$ (1.4)	Becker and Hassa (2002) Freitag and Hassa (2008)
	$q, We_g$	$\frac{y}{d_j} = \kappa q^\alpha \left[ \psi \ln \left( \frac{x}{d_j} \right) + \xi \right] We_g^\beta$ (1.5)	Thawley et al. (2008) Wang et al. (2011)
	$q$	$\frac{y}{d_j} = \kappa q^\alpha \left[ 1 - \exp \left( \beta \frac{x}{d_j} \right) \right] \left[ 1 + \psi \exp \left( \gamma \frac{x}{d_j} \right) \right] \left[ 1 + \xi \exp \left( \delta \frac{x}{d_j} \right) \right]$ (1.6)	Chen et al. (1993) Elshamy et al. (2007)
$\frac{z}{d_j}$	$q$	$\frac{z}{d_j} = \kappa q^\alpha \left(\frac{x}{d_j}\right)^\beta$ (2.1)	Inamura et al. (1993) Song et al. (2011)
	$q$	$\frac{z}{d_j} = \kappa q^\alpha \ln \left[ 1 + \left( \beta \frac{x}{d_j} \right) \right]$ (2.2)	Oda et al. (1994)
$\frac{x_{BU}}{d_j}$	Constant	$\frac{x_{BU}}{d_j} = \kappa$ (3.1)	Iyogun et al. (2006) Lee et al. (2007)
	$q$	$\frac{x_{BU}}{d_j} = \kappa q^\alpha$ (3.2)	Schetz and Padhye (1977)
	$q$ , other	$\frac{x_{BU}}{d_j} = \kappa q^\alpha Z_1^\beta Z_2^\eta$ (3.3)	Bellofiore et al. (2007) Ragucci et al. (2007)
$\frac{y_{BU}}{d_j}$	$q$	$\frac{y_{BU}}{d_j} = \kappa q^\alpha$ (4.1)	Wu et al. (1997a) Zheng and Marshall (2011)
	$q$ , other	$\frac{y_{BU}}{d_j} = \kappa q^\alpha Z_1^\beta$ (4.2)	Bellofiore et al. (2007) Ragucci et al. (2007)

**Table 2**

Range of parameters considered in this study and corresponding non dimension numbers.

$d_j$ (cm)	20–60	$q$	4.3–39
$v_j$ (m/s)	5–15	$We_g$	$[1.6 - 5.29] \times 10^4$
$u_g$ (m/s)	50–90	$We_j$	$[1.39 - 12.5] \times 10^5$
$\rho_g$ (kg/m <sup>3</sup> )	1.18	$Re_g$	$[0.89 - 2.66] \times 10^6$
$\sigma$ (N/m)	0.072	$Re_j$	$[2.24 - 6.73] \times 10^6$
$g$ (m/s <sup>2</sup> )	9.81	$Oh_j$	$[1.35 - 2.34] \times 10^{-4}$
$p_g$ (Pa)	101325	$Bo_j$	$[0.54 - 4.89] \times 10^4$
$T$ (K)	300	$\rho^*$	846
$\mu_j$ (Pa s)	$8.89 \times 10^{-4}$	$\mu^*$	48
$\mu_g$ (Pa s)	$1.86 \times 10^{-5}$	$I_j$	0.01–0.2
$\rho_j$ (kg/m <sup>3</sup> )	997.6		

**Table 3**

Cases investigated in this study along with numerical (mesh refinement  $\Delta x$ , liquid jet turbulence level  $\epsilon_j$ , turbulence modeling) and physical (injector nozzle diameter  $d_j$ , liquid jet velocity  $v_j$ , gaseous crossflow velocity  $u_g$ ) parameters as well as corresponding non-dimensional numbers. Case 1 is chosen as the case of reference. Highlight in yellow the parameters changed with respect to the reference case Case 1.

Case	Legend in figures	Numerical parameters			Physical parameters			Non dimension numbers				
		$\Delta x$ [mm]	$I_j$	RANS	$d_j$ [cm]	$v_j$ [ms <sup>-1</sup> ]	$u_g$ [ms <sup>-1</sup> ]	$q$	$Re_j \times 10^6$	$Re_g \times 10^6$	$We_g \times 10^4$	$We_j \times 10^5$
1	— + —	16	0.01	$k - \epsilon$	40	10	70	17.3	4.9	1.78	3.2	5.54
2	— + —	30	0.01	$k - \epsilon$	40	10	70	17.3	4.9	1.78	3.2	5.54
3	— + —	50	0.01	$k - \epsilon$	40	10	30	17.3	4.9	1.78	3.2	5.54
4	— + —	70	0.01	$k - \epsilon$	40	10	70	17.3	4.9	1.78	3.2	5.54
5	— • —	16	0.2	$k - \epsilon$	40	10	70	17.3	4.9	1.78	3.2	5.54
6	— × —	16	×	×	40	10	70	17.3	4.9	1.78	3.2	5.54
7	— △ —	16	0.01	$k - \omega$	40	10	70	17.3	4.9	1.78	3.2	5.54
8	— □ —	16	0.01	$k - \epsilon$	20	10	70	17.3	2.24	0.89	1.6	2.77
9	— * —	16	0.01	$k - \epsilon$	60	10	70	17.3	6.73	2.66	4.8	8.31
10	— ▽ —	16	0.01	$k - \epsilon$	40	5	70	4.3	2.24	1.78	3.2	1.39
11	— ★ —	16	0.01	$k - \epsilon$	40	7	70	8.5	3.14	1.78	3.2	2.72
12	— ▷ —	16	0.01	$k - \epsilon$	40	15	70	39	6.73	1.78	3.2	12.5
13	— ◇ —	16	0.01	$k - \epsilon$	40	10	50	33.9	4.9	1.27	1.63	5.54
14	— ○ —	16	0.01	$k - \epsilon$	40	10	90	10.5	4.9	2.28	5.29	5.54



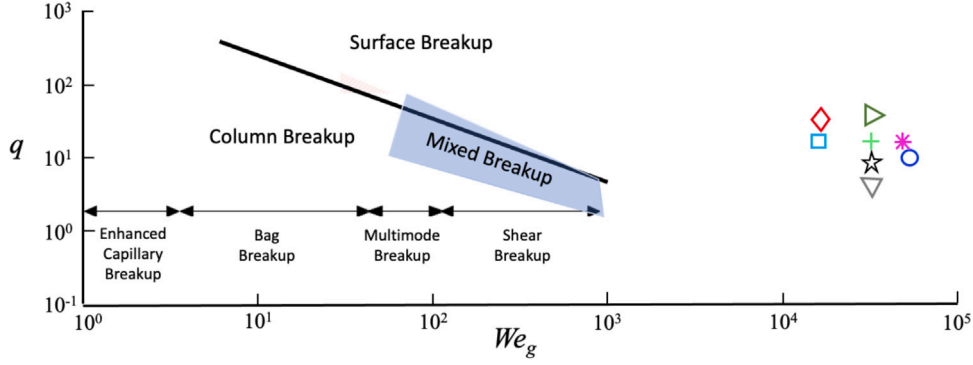


Fig. 2. Cases considered in this study reported in the  $We_g - q$  map adapted from Madabhushi et al. (2006). The continuous line is the transition between SBU and CBU from Wu et al. (1997a). Symbols are the simulations performed in this study as defined in Table 3.

The parameters  $q$  and  $We_g$  considered in this study are compared in Fig. 2 to the parameters  $q$  and  $We_g$  considered in previous studies. As shown the range of momentum ratio  $q$  is quite similar to what have been investigated so far and corresponds to a region where a mixed breakup regime (Column and surface) is expected. However, the use of an injection diameter more than two orders of magnitude larger induces much larger Weber numbers.

### 3. Numerical method

#### 3.1. Governing equations and numerical methods

The numerical simulations were performed with a finite volume approach, using the CFD code Star-ccm+ (Siemens, 2015). Here, we solve the unsteady, three-dimensional and incompressible Navier–Stokes equation for a Newtonian fluid:

$$\frac{\partial u_i}{\partial x_i} = 0 \quad (3)$$

$$\rho \frac{\partial u_i}{\partial t} + \rho u_j \frac{\partial u_i}{\partial x_j} = -\frac{\partial p}{\partial x_i} + \mu \frac{\partial}{\partial x_j} \left( \frac{\partial u_i}{\partial x_j} + \frac{\partial u_j}{\partial x_i} \right) - g \delta_{i2} + F_{\sigma i} \quad (4)$$

where  $u_i$ ,  $p$ ,  $\rho$ ,  $\mu$  and  $g$  stand for the velocity field, the pressure, the density, the viscosity and the gravity, respectively. The components of the velocity field  $u_i$  are noted  $u$ ,  $v$  and  $w$  along the  $x$ -,  $y$ - and  $z$ - directions, respectively. The surface tension force  $F_\sigma$  located at the interface between the two phases is expressed using the Continuum Surface Force (CSF) method (Brackbill et al., 1992) in the framework of the Volume of Fluid (VoF) method (Hirt and Nichols, 1981):

$$F_{\sigma i} = \sigma \kappa \frac{\partial \chi_i}{\partial x_i}, \quad \kappa = -\frac{\partial n_i}{\partial x_i}, \quad \vec{n} = \frac{\vec{\nabla} \chi}{\|\vec{\nabla} \chi\|} \quad (5)$$

where  $\sigma$  is the surface tension,  $\kappa$  is the mean interface curvature expressed in terms of the unit normal vector  $\vec{n}$  of the liquid–gas interface and  $\chi$  is the VoF function defined as  $\chi = 1$  in the liquid and  $\chi = 0$  in the gas. Density and dynamic viscosity are thus calculated as:

$$\rho = \rho_j \chi + \rho_g (1 - \chi), \quad \mu = \mu_j \chi + \mu_g (1 - \chi) \quad (6)$$

and  $\chi$  is transported by solving

$$\frac{\partial \chi}{\partial t} + u_i \frac{\partial \chi}{\partial x_i} = 0 \quad (7)$$

Different values of  $\chi$  will be considered to discuss the liquid column evolution. The value  $\chi = 0.9$  indicates that there is more than 90% of liquid in the controlled volume. It will be considered in order to characterize the liquid core, while  $\chi = 0.1$  (and lower values) will be used to discuss the envelop of the liquid cloud once atomized and dispersed in the air.  $\chi = 0.5$  will be also considered because corresponding to the interface location in fully resolved regions.

A finite volume method has been employed in order to discretize this system of equations together with a segregated multiphase flow

solver implemented in Star-ccm+ on a collocated (non-staggered) variable arrangement grid (Siemens, 2015). The solver uses a Rhie–Chow interpolation type velocity–pressure coupling in combination with a SIMPLE algorithm (Patankar and Spalding, 1972) based on pressure correction methods. The SIMPLE algorithm has been chosen here as the best compromise between numerical stability, computational time and accuracy. The SIMPLE algorithm is known for its robustness and is well adapted for integrating the RANS modeling of turbulence. The main objective of our study is to access to the large-scale liquid column fragmentation. Both grid resolution and selected time step do not allow to capture the fast breakup mechanisms at scales smaller than the grid size. However, the column breakup and the induced long arm and leg like structures as described in the following are slower process that can be captured by both the grid and time resolutions used for this study. In this context the SIMPLE model is a good compromise as usually recommended for slow transient simulation with relatively large time steps.

The liquid jet turbulence has been observed to impact the primary atomization for liquid jet at small scale (Lee et al., 2007; Osta and Sallam, 2010; Broumand and Birouk, 2017). As a first step in the investigation of large-scale liquid jet fragmentation, a RANS approach is considered here. A Realizable  $k - \epsilon$  model (Shih et al., 1995) is selected together with the VOF model. A two layers wall treatment is used in combination with the Realizable  $k - \epsilon$  model. In order to investigate turbulence modeling impact on the solution, the use of the Menter’s SST  $k - \omega$  (F.R., 1994) turbulence model has been concurrently analyzed as it is supposed to be more accurate for free shear flows and separated flows. According to the turbulence model selected, two equations describing turbulent quantities are added to the previous set of equations, being about turbulent kinetic energy  $k$  and either turbulent dissipation rate  $\epsilon$  or a characteristic turbulent frequency  $\omega$ , for  $k - \epsilon$  and  $k - \omega$  models respectively.

A second order High Resolution Interface Capturing (HRIC) discretization scheme has been used in Eq. (7) ensuring a sharp interface between the two phases and limiting its smearing by numerical diffusion (Muzafarjia and Peric, 1998). A second order upwind schemes were employed for convective terms in momentum and turbulent transport equations, while a first order implicit scheme was applied to the temporal discretization enhancing numerical stability. A time step of  $\Delta t = 1 \times 10^{-3}$  s has been used yielding to Courant–Friedrichs–Lewy numbers  $CFL$  ranging in  $3.2 \leq CFL \leq 5.7$ . Both the selected grid resolution (see next section) and time step do not allow to capture the fast breakup mechanisms at scales smaller than the grid size. Our main interest is here to investigate the large scale fragmentation of the injected liquid. The characteristic time for the injected liquid to reach the CBU point can be estimated (see Section 4.4) as  $y_{BU}/v_j \approx 10 d_j/v_j \approx 0.4$ s, requiring 400 time steps.

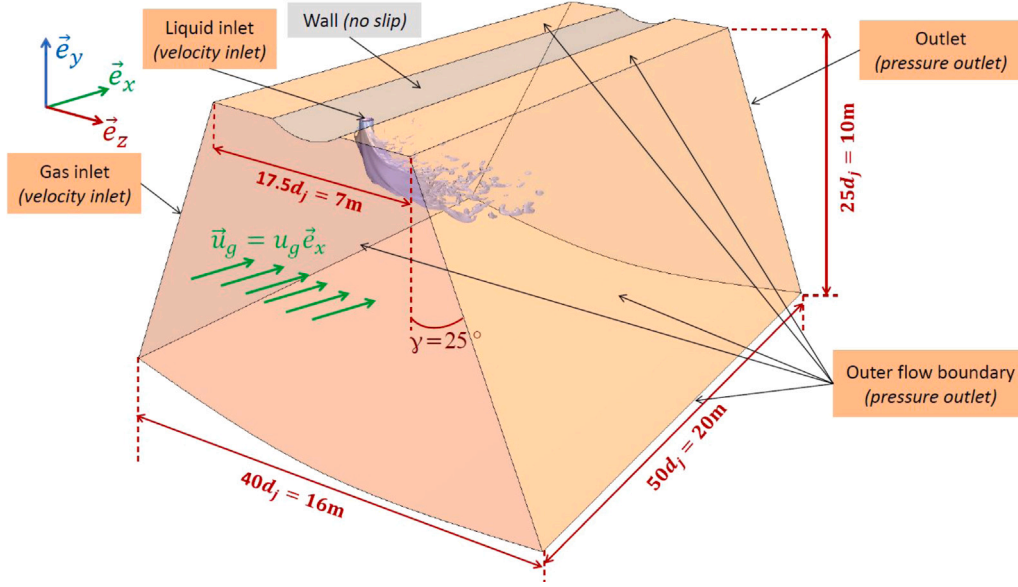


Fig. 3. Computational domain shape and main dimensions for the reference case 1 together with the imposed boundary conditions.

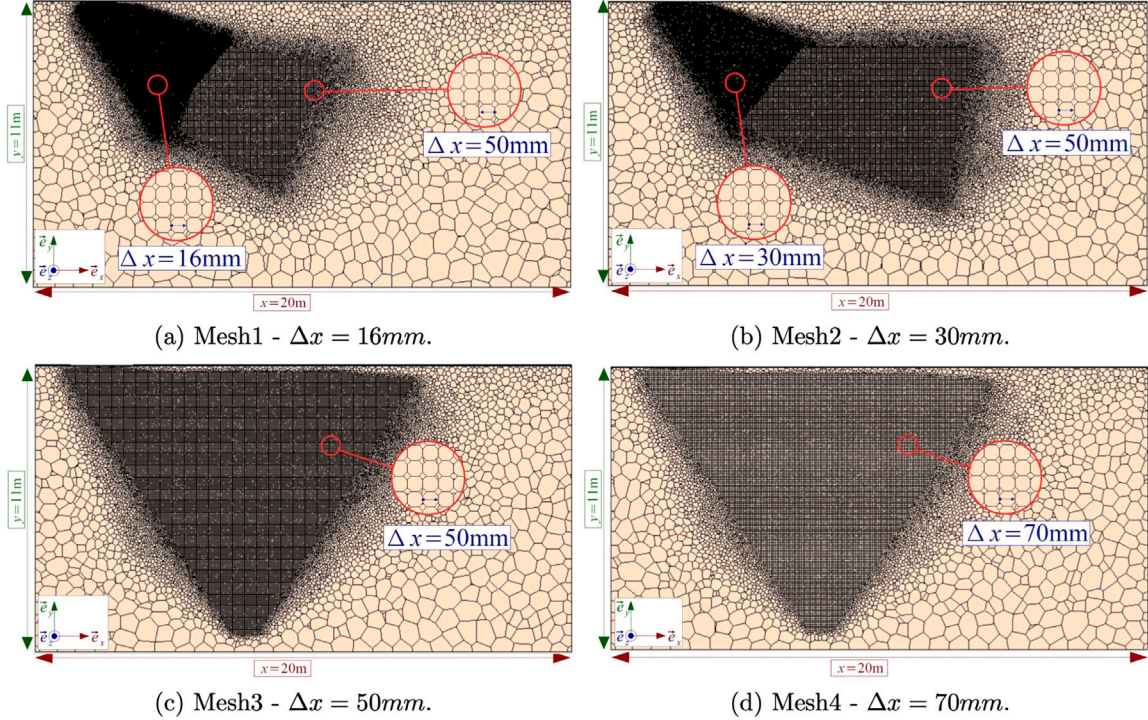


Fig. 4. A vertical slice of the meshes at  $z/d_j = 0$  showing the mesh refinement used to capture the liquid jet zone.

### 3.2. Computational domain and boundary conditions

Fig. 3 shows the computational domain and the main dimensions for the reference case 1 (see Table 3) together with the imposed boundary conditions. In order to minimize the number of cells, a trapezoidal domain is built from a rectangular surface of  $50d_j \times 17.5d_j$  at the top of the computational domain in the horizontal streamwise  $x$  and spanwise  $z$  directions, respectively. Instead of a classic flat plate usually used in LJGC numerical studies, a curved shape wall is considered to characterize an airplane lower surface (Bury et al., 2008). However, It has been observed with some preliminary tests not reported here that this curved shape of the top wall does not affect significantly the jet

evolution in comparison to a flat plate. The vertical direction of the domain is about 25 times the injector diameter and the trapezoidal geometry with an opening angle  $\gamma = 25^\circ$  ends with an equivalent rectangular surface of  $50d_j \times 40d_j$  at the bottom of the computational domain.

The top wall is considered as a no-slip boundary condition and a uniform inlet liquid velocity  $v_j$  is imposed at the nozzle exit. A uniform gas velocity  $u_g$  is imposed at the domain inlet. The other boundaries are considered as outflow domain boundaries with a pressure outlet fixed to the atmospheric pressure. The distance between the beginning of the computational domain at the gas inlet surface and the location of the center of liquid jet injector nozzle is set to  $l = 2.5$  m for all this study.

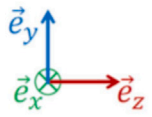
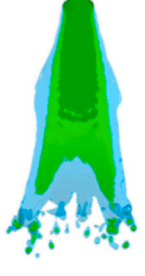



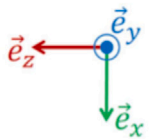




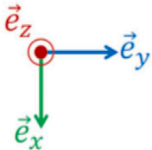




	Baseline	Coarse	Medium	Fine
$\Delta x$ [mm]	70	50	30	16
$d_j/\Delta x$	5.71	8	13.3	25
 Front view				
 Top view				
 Side view				

Fig. 5. Influence of the mesh refinement  $\Delta x$  on the shape of the liquid jet at  $t = 4.5$  s for several views and for different liquid volume fractions  $\chi$  (blue :  $\chi = 0.1$  , green :  $\chi = 0.5$  and red :  $\chi = 0.9$  ). (For interpretation of the references to color in this figure legend, the reader is referred to the web version of this article.)

The total simulated physical time in each case was about  $t = 5$  s ensuring the liquid jet to reach an established regime, i.e. a stabilized liquid penetration and transverse expansion.

### 3.3. Mesh convergence

This study used an unstructured mesh with polyhedral elements together with a prism layer remesher using 5 prism layers cells and a growth rate of 1.1 in order to take into account the boundary layer induced by the no slip condition at the wall. An hybrid-Gauss LSQ method is implemented for the gradient calculation throughout the unstructured mesh together with a gradient limiter using the Vankatakrishnan slope limiter scheme (V., 1993).

In order to find the best compromise between accuracy and computational speed, a mesh convergence study has been achieved. Four different meshes have been considered with different grid size  $\Delta x = 70$  mm,  $\Delta x = 50$  mm,  $\Delta x = 30$  mm and  $\Delta x = 16$  mm respectively for Mesh4 (Fig. 4d), Mesh3 (Fig. 4c), Mesh2 (Fig. 4b), and Mesh1 (Fig. 4a). The same time step  $\Delta t$  is used by varying the CFL condition. The mesh construction has been made in several steps. The objective is to be able to refine the region of interest while saving CPU time. First, a conventional rectangular computational domain (not shown here) with a regular coarse grid is used to determine the envelop of the liquid

jet trajectory. Then a trapezoidal shape that captures the full liquid jet evolution is defined resulting in Mesh4 shown in Fig. 4d with a grid size of 70 mm. Mesh3 in Fig. 4c is then obtained by refining this trapezoidal region with a grid size of 50 mm. Considering the obtained jet evolution in this mesh, the region that needs to be further refined is reduced while refining the mesh close to the exit resulting in Mesh2 and Mesh1 with grid size 30 mm and 16 mm shown in Figs. 4b and 4a, respectively.

Fig. 5 reports liquid column shape at time  $t = 4.5$  s for different views and for different refinement  $\Delta x$ . The different liquid volume fractions  $\chi = 0.9$ ,  $\chi = 0.5$  and  $\chi = 0.1$  are shown. Increasing the refinement clearly improves the resolution of the liquid core. In particular, the surface deformation results in elongated legs-like structures that originate from the nozzle, and the liquid cloud region ( $\chi = 0.1$ ) appears to be shaped by this legs-like structures with the development of detached liquid volume of big size. This will be depicted in more details in the following.

Fig. 6a and Fig. 6(b) report the corresponding vertical liquid column penetration  $y$  and transverse expansion  $z$  as a function of the stream-wise position  $x$ . The liquid cloud  $\chi = 0.1$  is shown since a priori more sensitive to the resolution than the liquid core  $\chi = 0.9$ . As observed the liquid column vertical penetration  $y$  does not seem to be sensitive to the resolution for the refinements considered here. The liquid transverse expansion  $z$  is found to be more sensitive to the grid resolution but a



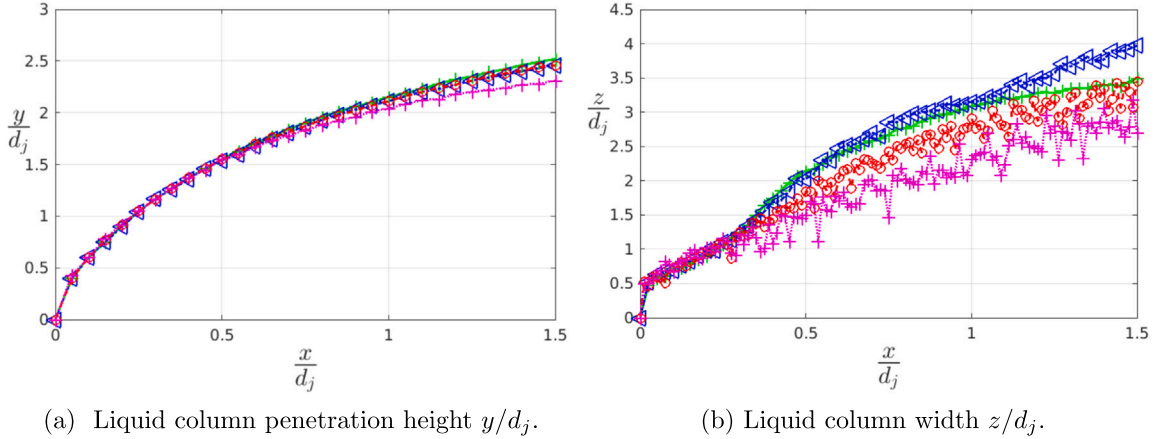


Fig. 6. Liquid column penetration height  $y/d_j$  and width  $z/d_j$  versus streamwise distance from the injector nozzle center  $x/d_j$  for  $\chi = 0.1$  and for several mesh refinement  $\Delta_x$  with:  $\cdot$   $\cdot$  Mesh1 ( $\Delta x = 16$  mm),  $\triangleleft$  Mesh2 ( $\Delta x = 30$  mm),  $\circ$  Mesh3 ( $\Delta x = 50$  mm),  $+$  Mesh4 ( $\Delta x = 70$  mm).

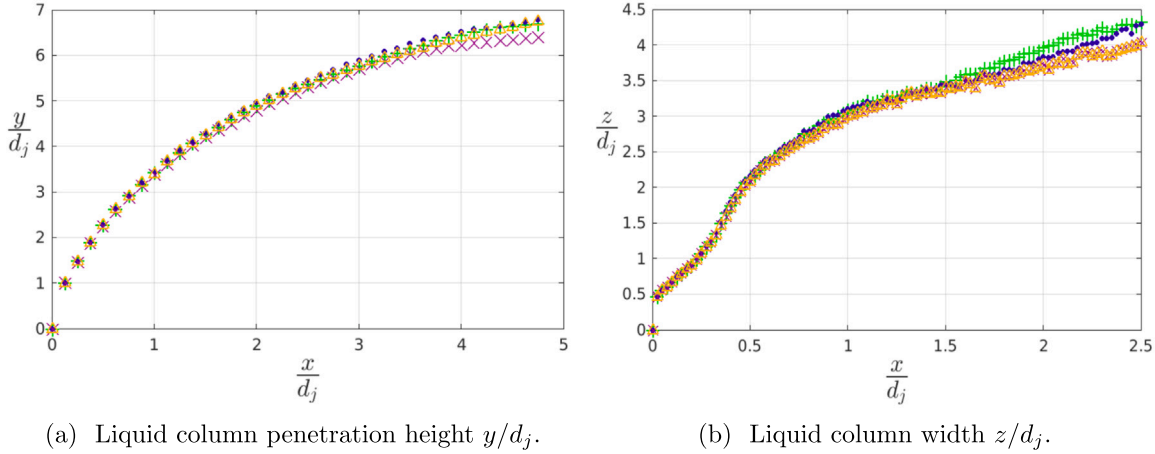


Fig. 7. Liquid column penetration height  $y/d_j$  and width  $z/d_j$  versus horizontal distance from the injector nozzle  $x/d_j$  for several turbulence models and turbulence intensity level  $I_j$  with: Case 1  $\cdot$   $\cdot$   $I_j = 0.01$ ,  $k-\epsilon$  model, Case 5  $\triangleleft$   $I_j = 0.2$ ,  $k-\epsilon$  model, Case 6  $\times$  without turbulence model, Case 7  $\triangle$   $I_j = 0.01$ ,  $SST-k-\omega$  model.

grid convergence seems to emerge from the reported evolutions. Note that the convergence is more difficult to reach at the jet lateral sides. In this region refining the grid results in a more accurate description of the shear breakup that would require finer meshes for a consistent resolution of the resulting droplets. In terms of CPU time, the finer mesh is eight times more consuming than the coarser mesh. Finally, the finer mesh has been selected for this study and the results reported in the following have been obtained with the fine mesh with  $\Delta x = 16$ . Thus, liquid droplets larger than several  $\Delta x = 16$  mm, typically with size  $O(50)$  mm, and their deformation and fragmentation are captured by the simulation. Smaller droplets cannot be properly resolved but they contribute to the liquid cloud. They are described by values of  $\chi$  lower than 1 and thus transported and dispersed by the flow with the resolution of Eq. (7).

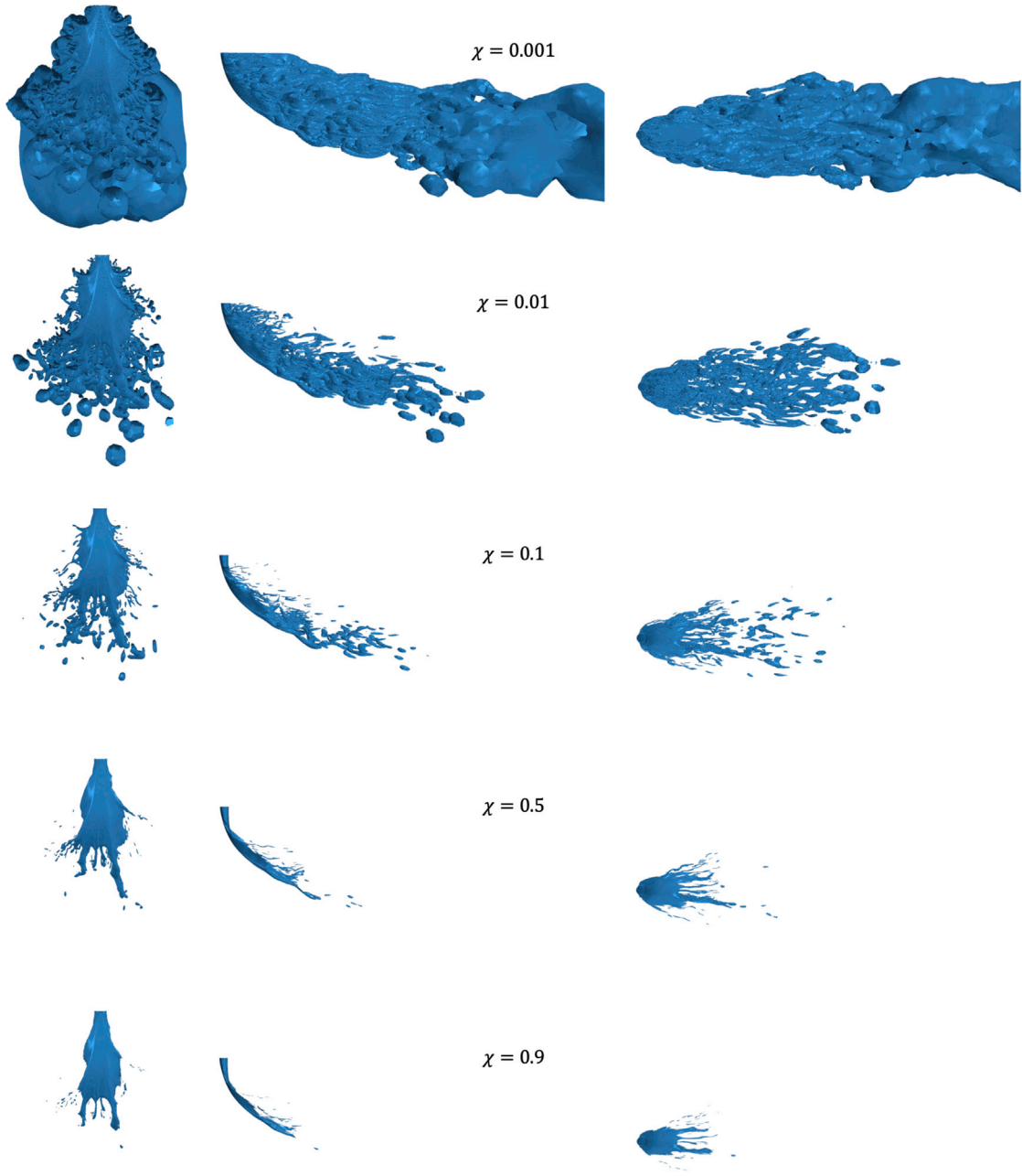
### 3.4. Turbulence modeling impact

Considering the high values of the Reynolds numbers of both the liquid jet and the air flow motion, some tests have been conducted on the turbulent modeling to be used in the simulations. For that purpose, different liquid jet turbulence intensity levels  $I_j$  and different turbulence models have been compared. The corresponding liquid jet evolutions for different views and different liquid volume fractions  $\chi$  are shown in Fig. 18 in Appendix A.1. Qualitatively speaking, the numerical simulations give few differences. This is confirmed with Fig. 7

where the corresponding liquid column penetration  $y$  and transverse expansion  $z$  are reported. When deactivating the RANS turbulence model in the set of equations to be solved (Case 6), the penetration of the liquid jet in the air crossflow tends to slightly decrease in comparison to the simulations carried out with different turbulent intensities and turbulent solvers. The range of the turbulent intensity of the liquid at the nozzle  $I_j$  investigated here does not seem to have a significant impact on both the vertical penetration and transverse expansion. Note that a simulation considering the LES approach has also been compared to the RANS simulations reported here and no significant difference has been observed. The choice of the turbulent model does not also seem to have an important impact on these two quantities. Because of its lower computational cost and its suitability with VOF method (Zhu et al., 2021), the Realizable  $k-\epsilon$  model is a fair compromise and was chosen for the numerical investigation presented here.

## 4. Results

The objective of the numerical investigation reported in this paper is to describe the liquid column atomization at large scale in a region close to the injection. For that purpose, we investigate the effects of the main parameters of the problem (liquid ejection velocity, nozzle diameter and airflow velocity) on the liquid evolution in the air cross flow under well controlled conditions and with fixed physical parameters (viscosities, densities and surface tension). The shape of the liquid column is described and the liquid vertical penetration and its



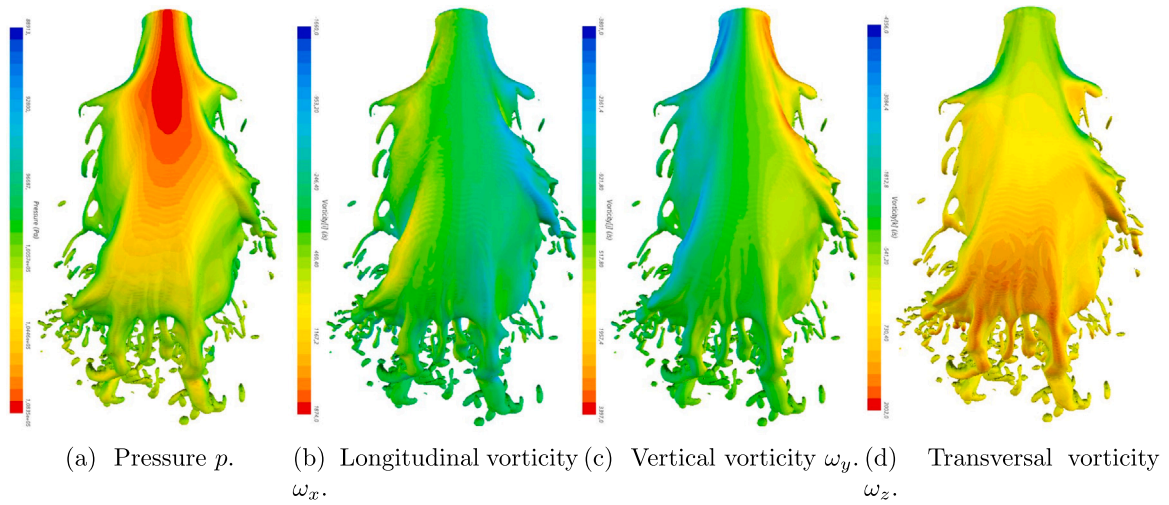
**Fig. 8.** Liquid column for different views and for different level of  $\chi$  at  $t = 4.5$  s for the reference case ( $q = 17.3$  and  $We_g = 3.2 \times 10^4$ ). (left) front view, (center) side view, (right) top view.

transverse expansion are reported and compared with results obtained for liquid jet at much smaller scale.

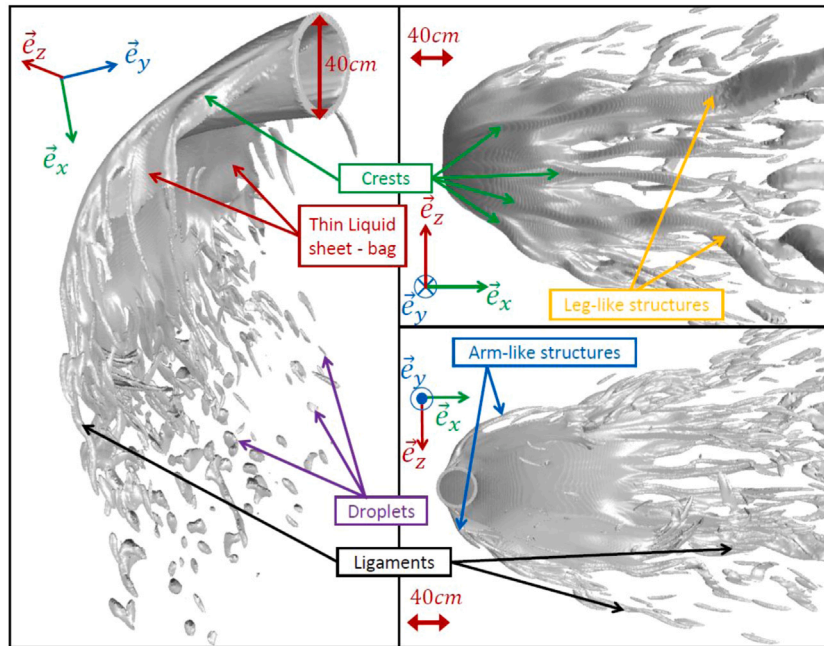
#### 4.1. Liquid column deformation and fragmentation

**Fig. 8** reports the shape of the liquid column for the reference case (Case 1),  $q = 17.3$  and  $We_g = 3.2 \times 10^4$ , at time  $t = 4.5$  s. The front, side and top views of the liquid column are reported. In order to investigate the liquid column structure, different levels of  $\chi$  are shown from the liquid cloud  $\chi = 0.001$  up to the liquid core  $\chi = 0.9$ . A behavior very similar to millimetric liquid jet is observed for both the liquid column trajectory but some specificity can be pointed out regarding its fragmentation. The liquid column is deflected along the streamwise direction due to the high pressure resulting from the impact of the air cross flow (as illustrated with the pressure distribution on the liquid column in **Fig. 9**) creating a stagnation point in the

oncoming gas flow together with the formation of a low pressure wake region on its downward surface (**Inamura, 2000**). This upstream-downstream pressure difference induces an aerodynamic drag exerted by the gaseous crosswind on the liquid jet (as characterized in **Fig. 9** with the vorticity components), gradually inducing the liquid column to bend along its trajectory causing it to be aligned with crossflow direction far away from the nozzle. As shown in **Fig. 8**, when comparing the different level of the VoF function  $\chi$ , the liquid column atomization reveals the presence of both the Column Breakup (CBU) and the Surface (or shear) Breakup (SBU) mechanisms. We observe the production of relatively large liquid fragments with ligament and droplet-like shape. The location of the CBU point can be clearly identified when considering the value  $\chi = 0.9$ . Comparing the iso-value  $\chi = 0.9$  to the lower iso-values  $\chi = 0.001, 0.01$  and  $0.1$  a cloud of droplet of size much smaller than the grid resolution is produced revealing a strong effect of the SBU mechanism.



**Fig. 9.** Front view of (a) the pressure field, (b) the streamwise vorticity, (c) the vertical vorticity and (d) the spanwise vorticity on the so-called liquid cloud surface ( $\chi = 0.1$ ) at  $t = 4.5$  s for the reference case (Case 1)  $q = 17.3$  and  $We_g = 3.2 \times 10^4$ .



**Fig. 10.** Liquid jet main structures for different views of the liquid cloud ( $\chi = 0.1$ ) at  $t = 4.5$  s for the reference case ( $q = 17.3$  and  $We_g = 3.2 \times 10^4$ ).

The simulations show that the specificity of the fragmentation at such scale is the production of long legs of liquid aligned with the air flow. Fig. 10 depicts the main large scale structures of the liquid jet from different perspectives. This case is very representative of all the cases considered in this study. Two main structures are observed on the liquid column shape: crests subsequently giving birth to ligaments and droplets as well as relatively thin liquid sheets (or bag) taking birth inside the troughs located between two consecutive crests. The wave length between two crests has the same order of magnitude than the injector size. Those two main types of structures are due to the strong shear rate experienced in the close vicinity of the interface between gas and liquid phases. Crests may give birth to arm-like structures all along the liquid column sides on the upper part, and they also induce several well pronounced leg-like structure on its lower part. The original aspect observed for large liquid jet as considered in our study is certainly the development of several very long arm and leg like structures. This is clear when comparing for example Fig. 10 with Fig. 20 in Zhu et al. (2021) and with Fig. 16, 17 and 20 in Behzad et al. (2016). The arm-like

and leg-like structures produce both ligaments and droplets, though the former yielding to relatively smaller detached structures than the latter. Both kind of crest structures are induced by the strong shear between the two phases as illustrated in Fig. 9 with the vorticity components, and they are then stretched out by the air crossflow producing thus the liquid spray at the end of the fragmentation cascade and their development along the azimuthal direction. Interestingly, a clear similarity appears here at large scale when compared to the literature for smaller size jets. While our description of liquid column arm-like structures is related to stripping-off mechanisms, leg-like structures are associated to liquid column pinch-off. A detailed inspection of the liquid column surface in Fig. 10 indicates the presence of smaller scale corrugations very similar to the ones reported by Behzad et al. (2015) at much smaller nozzle size and as a consequence with a much better resolution when compared to the nozzle diameter.

As shown in Fig. 9(a), the ligaments-like (also called arm-like) structures all along the liquid column edges are characterized by lower pressure while relatively high values of the vorticity components are



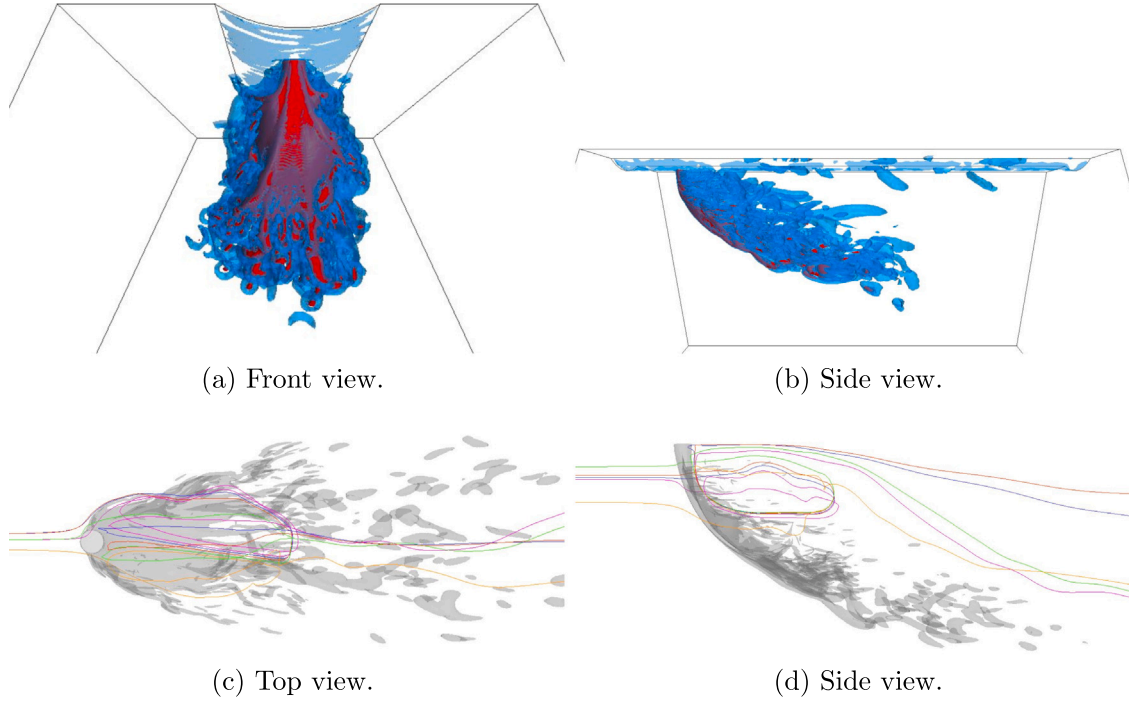


Fig. 11. Reference case  $q = 17.3$  and  $We_g = 3.2 \times 10^4$  at  $t = 4.5$  s. (First line) Visualization in blue of the iso-surface  $Q = 1000 \text{ s}^{-2}$  with in red the liquid cloud surface  $\chi = 0.1$ . (Second line) visualization of flow field pathlines with in gray liquid cloud surface  $\chi = 0.1$ . (For interpretation of the references to color in this figure legend, the reader is referred to the web version of this article.)

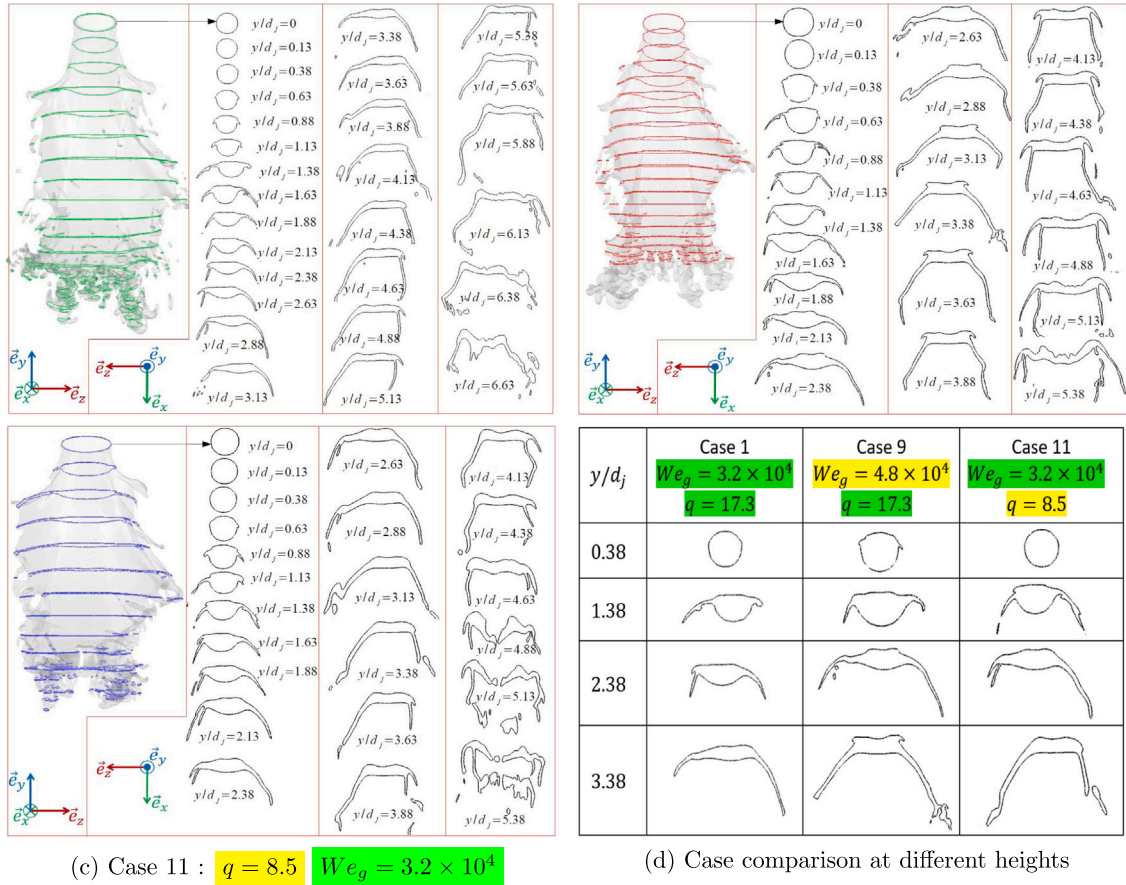
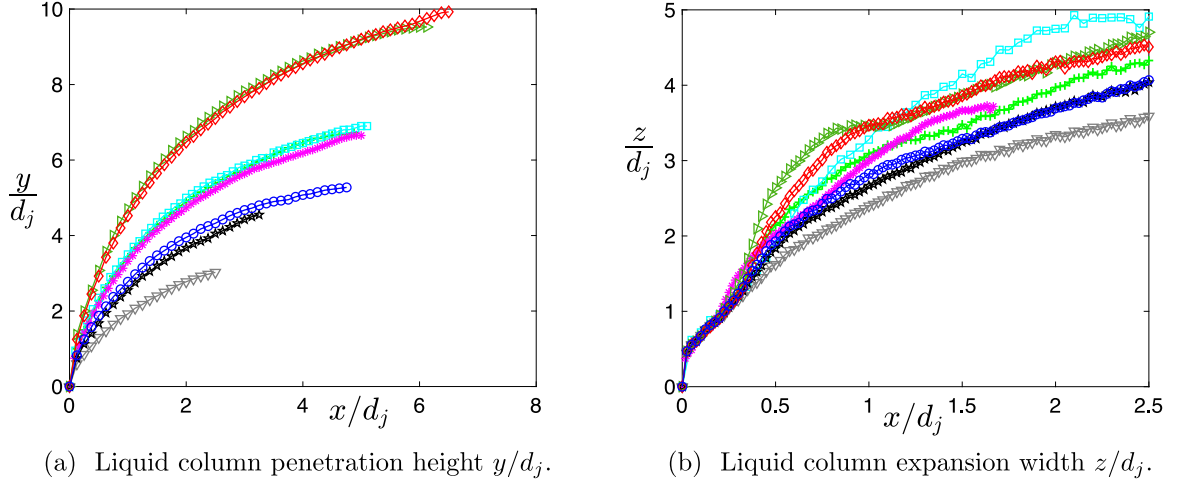
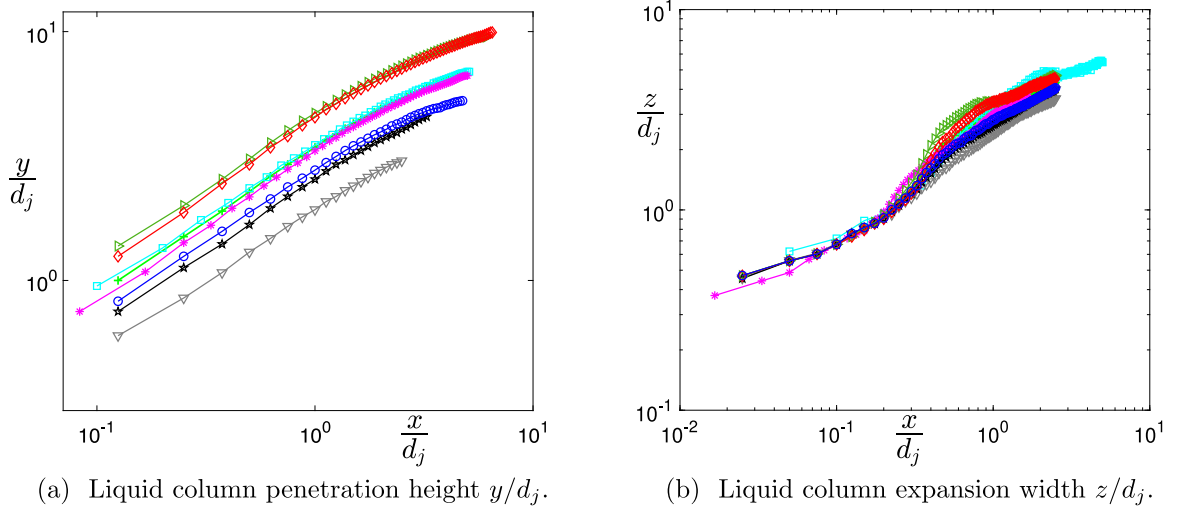


Fig. 12. Liquid jet cross section shape evolution for different penetration heights  $y/d_j$  and for different momentum ratio  $q$  and crossflow Weber number  $We_g$  for the liquid cloud ( $\chi = 0.1$ ) at  $t = 4.5$  s.





**Fig. 13.** Liquid column (a) normalized vertical penetration  $y/d_j$  and (b) normalized transverse expansion  $z/d_j$  versus the horizontal distance from the injector nozzle  $x/d_j$  for several crossflow Weber numbers  $We_g$  and momentum ratio  $q$ . Case 1 — + —  $We_g = 3.2 \times 10^4 - q = 17.3$ , Case 8 — □ —  $We_g = 1.6 \times 10^4 - q = 17.3$ , Case 9 — \* —  $We_g = 4.8 \times 10^4 - q = 17.3$ , Case 10 — ▽ —  $We_g = 3.2 \times 10^4 - q = 4.3$ , Case 11 — ★ —  $We_g = 3.2 \times 10^4 - q = 8.5$ , Case 12 — ▷ —  $We_g = 3.2 \times 10^4 - q = 39$ , Case 13 — ◊ —  $We_g = 1.63 \times 10^4 - q = 33.9$ , Case 14 — ◊ —  $We_g = 5.29 \times 10^4 - q = 10.5$ .



**Fig. 14.** Log-Log plot of the liquid column (a) normalized vertical penetration  $y/d_j$  and (b) normalized transverse expansion  $z/d_j$  versus the horizontal distance from the injector nozzle  $x/d_j$  for several crossflow Weber numbers  $We_g$  and momentum ratio  $q$ . Case 1 — + —  $We_g = 3.2 \times 10^4 - q = 17.3$ , Case 8 — □ —  $We_g = 1.6 \times 10^4 - q = 17.3$ , Case 9 — \* —  $We_g = 4.8 \times 10^4 - q = 17.3$ , Case 10 — ▽ —  $We_g = 3.2 \times 10^4 - q = 4.3$ , Case 11 — ★ —  $We_g = 3.2 \times 10^4 - q = 8.5$ , Case 12 — ▷ —  $We_g = 3.2 \times 10^4 - q = 39$ , Case 13 — ◊ —  $We_g = 1.63 \times 10^4 - q = 33.9$ , Case 14 — ◊ —  $We_g = 5.29 \times 10^4 - q = 10.5$ .

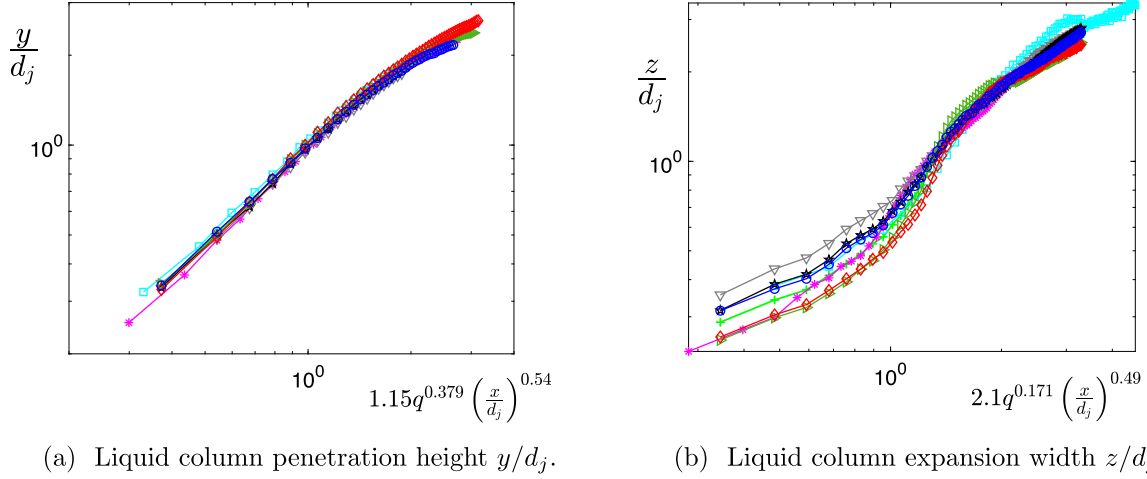
observed, which aims at stretching the liquid column along on the airstream direction and extending its area. Relatively high value of  $\omega_x$  and  $\omega_y$  are occurring on the crests of the liquid column sides where ligaments and droplets are generated,  $\omega_z$  reaches its maximum values on the windward surface and all along large elongated ligaments structures shaped close to the CBU location. Fig. 11 puts ahead the complex tridimensional vortices structures arising in the wake of the liquid column through the  $Q$  criterion iso-surface allowing to track vortical systems in the flow field. Those vortices closely connected to the low pressure region downstream the liquid column, induce a strong tridimensional recirculation region as also reported in Fig. 11.

Finally, as an important result, the simulations show that the penetration and the lateral expansion of the jet follow the same evolution as the millimeter jets for diameters of 3 orders of magnitude greater. Our simulations reveal that at large scale several long arm and leg structures develop and they significantly elongate along the streamwise direction.

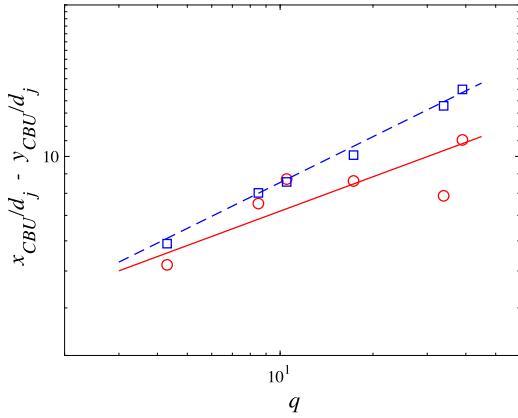
#### 4.2. Effect of the airflow velocity, liquid injection velocity and nozzle diameter

We now discuss the effect of the nozzle diameter, the liquid injection velocity and the airflow velocity on the liquid column evolution. The corresponding liquid jet evolutions for different views and different liquid volume fractions  $\chi$  are shown in Fig. 19 (Appendix A.2), in Fig. 20 (Appendix A.3) and Fig. 21 (Appendix A.4), respectively. Note that a change in  $d_j$  induces a variation in the air Weber number  $We_g$  only, a change in  $v_j$  induces a variation in the momentum ration  $q$  only, while a change in  $u_g$  yields to a variation in both  $We_g$  and  $q$ .

As observed in Fig. 19 (Appendix A.2), increasing  $d_j$  obviously increases the characteristic sizes of the liquid column considering its vertical penetration, transverse expansion and streamwise development. However, similar structures as detailed in the previous section for Case 1 are observed. The main difference is related to the twin “leg” structures more pronounced when decreasing the nozzle diameter, i.e. for both smaller airflow and liquid Weber number, while



**Fig. 15.** Evolutions reported as a function of their respective correlations. Case 1  $\text{---} + \text{---}$   $W e_g = 3.2 \times 10^4$ ,  $q = 17.3$ ,  $\text{---} \square \text{---}$   $W e_g = 1.6 \times 10^4$ ,  $q = 17.3$ , Case 9  $\text{---} * \text{---}$   $W e_g = 4.8 \times 10^4$  -  $q = 17.3$ , Case 10  $\text{---} \nabla \text{---}$   $W e_g = 3.2 \times 10^4$  -  $q = 4.3$ , Case 11  $\text{---} \star \text{---}$   $W e_g = 3.2 \times 10^4$  -  $q = 8.5$ , Case 12  $\text{---} \triangleright \text{---}$   $W e_g = 3.2 \times 10^4$  -  $q = 39$ , Case 13  $\text{---} \diamond \text{---}$   $W e_g = 1.63 \times 10^4$  -  $q = 33.9$ , Case 14  $\text{---} \circ \text{---}$   $W e_g = 5.29 \times 10^4$  -  $q = 10.5$ .



**Fig. 16.** Evolution of the streamwise distance  $x_{CBU}/d_j$  ( $\circ$ ) and vertical penetration  $y_{CBU}/d_j$  ( $\square$ ) as a function of the momentum ratio  $q$ .  $\text{---}$  relation (12),  $\text{---}$  relation (13).

“arm” structures are more developed, but with a reduced size, when increasing the diameter and thus the Weber number.

When increasing the liquid injection velocity (Fig. 20, Appendix A.3), the liquid column development is also observed to increase, with in particular a stronger liquid penetration. Similar structures are observed with no noticeable change in the “arm and leg” structure organization.

When increasing the airflow velocity (Fig. 21, Appendix A.4), the liquid jet penetration is clearly reduced while the transverse expansion is increased, but no noticeable change in the “arm and leg” structure is observed.

As shown, the development of the large scale structures “arm” and “leg” are clearly changing when varying the Weber number. The liquid column penetration and lateral expansion appears to be more dependent on the momentum ratio  $q$ . This is confirmed with the liquid column cross sections reported in Fig. 12. Fig. 12a, Fig. 12b and Fig. 12c report the cross sections when varying the momentum ratio  $q$  and the airflow Weber number  $W e_g$ , the momentum ratio being maintained fixed while the Weber number is changed and vice versa. Fig. 12d compares the cross section for the three cases at different vertical locations. A similar deformation process is observed for the three reported cases. As shown the section of the liquid column is significantly varying along the liquid column trajectory. In addition, gaseous air stream accelerates across liquid column sides when bypassing them, causing gas dynamic

pressure increase. This pressure decrease across the liquid column edges circumference causes its cross section to deform itself by spreading laterally. Note that capillary effects allowing eventually to stabilize and dampen this spanwise or lateral motion (Aalburg et al., 2005) cannot be observed here due to the grid resolution larger than the capillary length. This liquid column cross section shape being a perfect circular shape at the injection point is progressively deformed first in an ellipsoidal and flattened kidney-like shape (Cavaliere et al., 2003) increasing the projected or effective area in direct contact with the upcoming gas flow (Wu et al., 1997a; Mazallon et al., 1999), increasing the drag force experienced by the liquid column and the induced bending effect. This flattening further increases with the formation of a liquid layer ending with arm and then legs (Behzad et al., 2016; Li and Soteriou, 2016).

### 4.3. Liquid column vertical penetration and transverse expansion

The vertical liquid penetration  $y$  as well as the transverse (or lateral) expansion  $z$  of a liquid jet in an air cross flow have been extensively investigated in the literature but for nozzle size several orders of magnitude smaller than those considered in this work as discussed in Section 2.1. In addition, different methods have been used in the literature for their measurement, explaining some significant discrepancies in the resulting empirical correlations.  $y$  and  $z$  are determined here considering the liquid column surface  $\chi = 0.1$ .

Fig. 13 reports the normalized liquid column vertical and transverse penetration height and width  $y/d_j$  and  $z/d_j$ , respectively, as a function of the normalized streamwise direction  $x/d_j$  for all the considered cases. As observed for the liquid column shapes commented in the previous section, the vertical penetration is impacted by the change in the momentum ratio  $q$  while the airflow Weber number  $W e_g$  has a smaller impact. Clearly the vertical penetration increases when the momentum ratio increases, the jet inertia being stronger compared to the air flow inertia. The effect on the transverse expansion is less evident but a similar trend seems to emerge. Very close to the injection, the  $z$  evolution is only driven by the nozzle diameter  $d_j$ , and  $z \approx d_j$ . After this linear evolution, the jet expands in the transverse direction, and this expansion increases when increasing  $q$  due a stronger dispersion process.

In order to analyze how  $y/d_j$  and  $z/d_j$  evolve as a function of  $x/d_j$  a log-log representation is shown in Fig. 14. A clear power law evolution is observed for the liquid penetration corresponding to a scaling law of the form  $y \approx x^{\beta_y}$ . For the transverse expansion the behavior decomposes into two zones. In the first zone, as described above  $z \approx d_j$  for  $x/d_j <$

**Table 4**

Comparison between large diameter liquid column penetration height  $y/d_j$  and expansion width  $z/d_j$  with empirical correlations at small diameter issuing from literature.

Vertical penetration	$\frac{y}{d_j} = \kappa q^\alpha \left(\frac{x}{d_j}\right)^\beta$	$\kappa$	$\alpha$	$\beta$	$q$	$We_g$	$\frac{x}{d_j}$
This study	$1.146 q^{0.379} \left(\frac{x}{d_j}\right)^{0.54}$	1.146	0.379	0.54	4.3 – 39	16000 – 52900	0 – 6
Wu et al. (1997a)	$1.37 q^{0.5} \left(\frac{x}{d_j}\right)^{0.5}$	1.37	0.5	0.5	3.4 – 185	57 – 1180	0 – 12
Lin et al. (2002b)	$2.42 q^{0.48} \left(\frac{x}{d_j}\right)^{0.24}$	2.42	0.48	0.24	2 – 40	40 – 475	0 – 200
Iyogun et al. (2006)	$1.997 q^{0.444} \left(\frac{x}{d_j}\right)^{0.444}$	1.997	0.444	0.444	8.3 – 726	9.3 – 159	0 – 63.5
Yoon et al. (2011)	$2.29 q^{0.417} \left(\frac{x}{d_j}\right)^{0.429}$	2.29	0.417	0.429	2 – 29.1	5.3 – 47.9	0 – 27
Transverse expansion	$\frac{z}{d_j} = \kappa q^\alpha \left(\frac{x}{d_j}\right)^\beta$	$\kappa$	$\alpha$	$\beta$	$q$	$We_g$	$\frac{x}{d_j}$
This study	$2.1 q^{0.171} \left(\frac{x}{d_j}\right)^{0.489}$	2.1	0.171	0.489	4.3 – 39	16000 – 52900	0 – 6
Wu et al. (1997b)	$7.86 q^{0.17} \left(\frac{x}{d_j}\right)^{0.33}$	7.86	0.17	0.33	5.3 – 59.1	54 – 217	50 – 500
Inamura et al. (1993)	$1.4 q^{0.18} \left(\frac{x}{d_j}\right)^{0.49}$	1.4	0.18	0.49	×	×	×
Song et al. (2011)	$0.56 q^{0.4} \left(\frac{x}{d_j}\right)^{0.6}$	0.56	0.4	0.6	29 – 172	31	20 – 180

0.25 while for the second zone a power law evolution of the form  $z \approx x^{\beta_z}$  can also be proposed. Considering relations obtained for liquid jet at smaller scales, the evolution of the penetration and the transverse expansion with the streamwise direction should write in the form:

$$\frac{y}{d_j} = K_y q^{\alpha_y} \left(\frac{x}{d_j}\right)^{\beta_y} \quad (8)$$

$$\frac{z}{d_j} = K_z q^{\alpha_z} \left(\frac{x}{d_j}\right)^{\beta_z} \quad (9)$$

From the slope in Fig. 14 the values  $\beta_y = 0.54$  and  $\beta_z = 0.49$  are identified. Then the prefactor is reported in a log-log plot as a function of  $q$  and the values  $\alpha_y = 0.379$  and  $\alpha_z = 0.171$  are determined as well as the values  $K_y = 1.15$  and  $K_z = 2.10$ . Finally, the following evolutions of  $y/d_j$  and  $z/d_j$  are proposed as

$$\frac{y}{d_j} = 1.15 q^{0.379} \left(\frac{x}{d_j}\right)^{0.54} \quad (10)$$

$$\frac{z}{d_j} = 2.1 q^{0.171} \left(\frac{x}{d_j}\right)^{0.49} \quad \text{for } z \geq 0.25d_j \quad (11)$$

$y/d_j$  and  $z/d_j$  are reported in Fig. 15 as a function of their corresponding correlations given by Eqs. (10) and (11), respectively. As shown all the curves are now collapsing for both  $y/d_j$  and  $z/d_j$ . Of course the linear evolution  $z \approx d_j$  near the liquid exit ( $z \leq 0.25d_j$ ) cannot be described with the proposed scaling. The description of the transverse expansion could certainly be improved with the integration of the gas Weber number in the correlation as can be found in the literature. We have not found a convincing dependency and additional simulations would be necessary to cover a larger range of Weber numbers.

The values  $\beta_y = 0.54$ ,  $\beta_z = 0.49$ ,  $\alpha_y = 0.379$ ,  $\alpha_z = 0.171$ ,  $K_y = 1.15$  and  $K_z = 2.10$  able to describe with relations (10) and (11) the liquid vertical penetration and transverse expansion are compared in

Table 4 with power law scaling found in the literature for much smaller nozzle size. Facing the huge amount of empirical correlations available in literature (especially for penetration height), only correlations obtained for a similar range of momentum ratio  $q$  are reported. Despite a gas Weber number  $We_g$  much larger in the problem considered here (see Fig. 2), similar orders of magnitude are found for the coefficients.

#### 4.4. Liquid column breakup

We finally consider the location of the liquid column breakup CBU as defined in Fig. 1. The streamwise distance  $x_{BU}$  and vertical penetration  $y_{BU}$  have been defined as the mean values in time of the streamwise distance and vertical position of the liquid core ( $\chi = 0.9$ ) breakup. Their evolution with the momentum ratio  $q$  are reported in

Fig. 16 as a function of  $q$ . As shown they both increase with  $q$ . Most of the reported results of column breakup location in the literature indicate a constant value for the normalized streamwise position  $x_{BU}$  as reported in Table 5 for similar range of momentum ratio  $q$ . In our simulation  $x_{BU}/d_j$  is found to vary from 5 to 11 in agreement with the values reported in the table. Note that an increase of the normalized streamwise location  $x_{BU}/d_j$  has also been reported in experiments (Schetz and Padhye, 1977). From our results the following relation is proposed

$$\frac{x_{BU}}{d_j} = 3.6 q^{0.3} \quad (12)$$

A power law evolution for the vertical distance of the column breakup  $y_{BU}$  as a function of  $q$  can also be deduced from the simulations

$$\frac{y_{BU}}{d_j} = 3.4 q^{0.4} \quad (13)$$

When compared with previous results from literature we observe a smaller impact of  $q$  on the evolution of  $y_{BU}/d_j$ .

#### 4.5. Discussion

Up to our knowledge there is no experiments conducted for such large jet available for a direct comparison with our simulations. However a qualitative comparison can be made with water drop by the Boeing 747 of Evergreen and then Global Super Tanker companies.

The Boeing 747 was able to drop up to 70 m<sup>3</sup> of water or fire retardant at a pressure of 7 bars through four nozzles of 40 cm diameter located in line under the fuselage of the aircraft as shown in Fig. 17. Fig. 17 also reports the liquid column evolution for a water exit velocity of approx. 14 m/s. The aircraft velocity is around 70 m/s. The momentum ratio is then  $q = 33$  and the air Weber number is  $We_g = 3 \times 10^4$ . The correlations (10) and (11) deduced from our simulations for, respectively, the jet penetration and its lateral expansion are compared in photos showing the water column evolution under the airtanker. As observed the actual penetration is stronger compared to our simulations (red line), certainly due to the system made of 4 nozzles in line and the high level pressure used in the delivery system. However, the observed liquid column penetration can be satisfactorily reproduced (dash red line) by just replacing the prefactor  $K_y = 1.15$  by  $K_y = 2.8$  in Eq. (10). Considering now the lateral penetration, Eq. (11) (green line) correctly reproduces the transverse evolution of the liquid column considering the oblique angle of view of the photo.

Some additional information can be collected from the tests made for the certification of the Boeing 747. The liquid drop is made in 10 s resulting a liquid deposit on ground of 1 km long and 70 m width. The liquid ground pattern has been measured using the cup and grid

**Table 5**

Comparison between large diameter liquid column breakup streamwise  $x_{BU}/d_j$  and vertical  $y_{BU}/d_j$  obtained in our numerical simulation with empirical correlations at small diameter issuing from literature.

$x_{BU}$	$\frac{x_{BU}}{d_j} = \kappa q^\alpha$	$\kappa$	$\alpha$	$q$	$We_g$
This study	$3.6 q^{0.3}$	3.6	0.3	4.3 – 39	16000 – 52900
Wu et al. (1997a)	$8.06 \pm 1.46$	8.06	×	3.4 – 185	57 – 1180
Iyogun et al. (2006)	12	12	×	8.3 – 726	59.3 – 159
Thawley et al. (2008)	6.9	6.9	×	1 – 54	9 – 345
$y_{BU}$	$\frac{y_{BU}}{d_j} = \kappa q^\alpha$	$\kappa$	$\alpha$	$q$	$We_g$
This study	$3.4 q^{0.4}$	3.4	0.4	4.3 – 39	16000 – 52900
Wu et al. (1997a)	$3.07 q^{0.53}$	3.07	0.53	3.4 – 185	57 – 1180
Thawley et al. (2008)	$2.5 q^{0.53}$	6.9	×	1 – 54	9 – 345



**Fig. 17.** Boeing 747 transformed into an airtanker dropping water. The exit is made of four circular holes of 40 cm in line. The water exit velocity is around 14 m/s and the aircraft velocity relative to surrounding air is approx. 70 m/s. The red line is relation (10), red dashed line is relation (10) with the prefactor  $K_y = 2.8$  instead of  $K_y = 1.15$ . The green line is relation (11). Photos in the first line: Courtesy of Marsaly (2016). Photos in the second line: Courtesy of Dan Reese President Global Supertanker Services from 2018 to 2021. . (For interpretation of the references to color in this figure legend, the reader is referred to the web version of this article.)

method (Suter, 2002). The method consists in performing liquid drops in real conditions over a flat field with no vegetation but covered with cups regularly distributed following a grid. The liquid is dropped by the airtanker and it then deposits on the ground filling the cups. The cups are then collected and weighted in order to determine the distribution of the quantity of liquid on the ground. Several test series have been performed by the USDA Forest Service for the Boeing 747 and the resulting drop patterns have been analyzed (Legendre et al., 2014). A power law for the pattern width  $\lambda/d_j = 58 q^{0.2}$  as a function of the momentum ratio  $q$  has been identified for values of  $q$  ranging from  $q = 18$  to  $q = 42$ . We can notice that this power law evolution with  $q$  observed for the ground pattern width  $\lambda$  is remarkably close to the transverse evolution  $z \approx d q^{0.17}$  proposed by relation (10). This result seems to indicate that the evolution of the jet in a region close to the ejection system is shaping the final liquid deposit on ground as observed in Fig. 17 when considering the satisfactory agreement between relation (10) and the lateral expansion of the liquid column.

This information is of great interest for the use of CFD for airtanker performance optimization or for the design of the new generation of airtankers. Indeed a complete simulation for the liquid deposit would require a domain of size length 1000 m  $\times$  width 80 m  $\times$  height 100 m, inaccessible with today-available super computers. We show here that the analysis of the liquid column development in a close region under the airtanker is able to provide relevant information for the jet development.

## 5. Conclusion

Near nozzle field behavior of round water liquid jets injected through a large injector diameter  $d_j$ , ranging from 0.2 to 0.6 m, into an air crossflow is numerically investigated using the Volume of Fluid (VoF) method. The liquid jet to gas momentum ratio  $q$  is ranging from 4.3 to 39 with a gas Weber number  $We_g$  ranging from  $1.6 \times 10^4$  to  $5.29 \times 10^4$ . The large scale liquid water jet main properties, such as primary breakup process, liquid column penetration height, liquid column



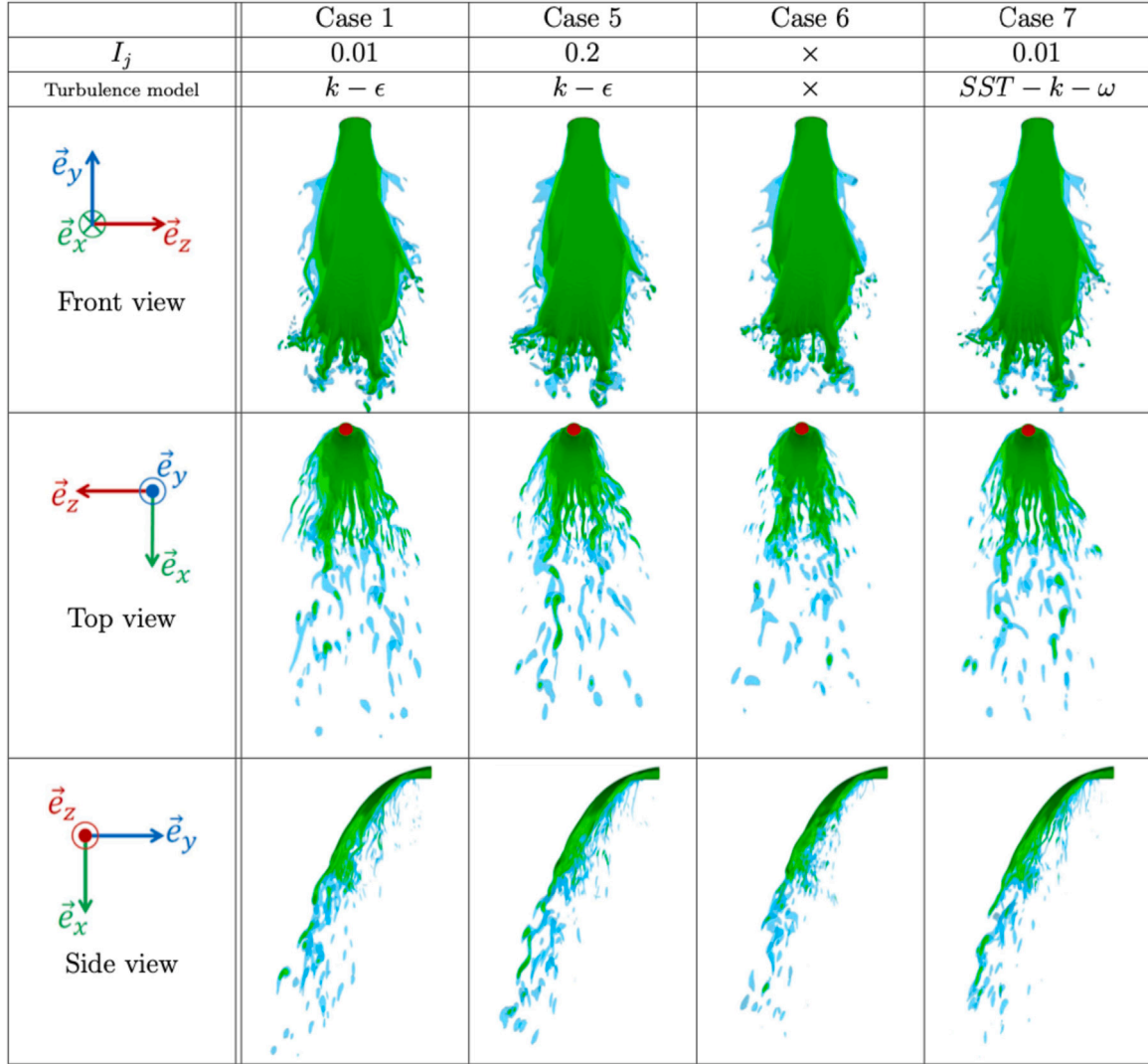


Fig. 18. Liquid jet turbulence intensity level  $I_j$  and turbulence model impacts on liquid jet shape during the flow field at  $t = 4.5$  s for several views and for different liquid volume fractions  $\chi_j$  (blue :  $\chi = 0.1$  , green :  $\chi = 0.5$  and red :  $\chi = 0.9$  ). (For interpretation of the references to color in this figure legend, the reader is referred to the web version of this article.)

expansion and column breakup point location have been investigated and compared to studies conducted for injectors of much smaller size. It has been found that the surface breakup mechanism (SBU) and column breakup mechanisms (CBU) are both contributing to the liquid column fragmentation. The fragmentation at large scale is characterized by the generation of a significant number of well pronounced leg and arm structures that align with the airflow at the end of the liquid column. Correlations for the main liquid jet properties are proposed and compared with previous results for smaller size liquid jet. Liquid column penetration height, width and column breakup height follow the same trend that those arising from empirical correlations at smaller size. No experimental results at such a large nozzle scale are available for a quantitative comparison, but the reported results are found to be consistent with liquid jet generated by the airtanker B747. When considering the application of our study to Aerial Fire Fighting, the ambient air can be at a significant higher temperature compared to the ejected liquid temperature resulting in liquid evaporation. This aspect will be the subject of future investigations.

## Nomenclature

### Acronyms :

LJGC :	Liquid Jet in Gaseous Crossflow
CBU :	Column Breakup
SBU :	Surface (or Shear) Breakup
VOF :	Volume of Fluid
CSF :	Continuum Surface Force
HRIC :	High Resolution Interface Capturing
SIMPLE :	Semi Implicit Method for Pressure Linked Equations

RANS :	Reynolds Averaged Navier Stokes
LES :	Large Eddy Simulation
PDPA :	Phase Doppler Particle Analyser
PIV :	Particle Image Velocimetry

### Subscripts :

$j$ :	Liquid jet (hereafter water)
$g$ :	Gaseous crossflow (hereafter air)
$BU$ :	Breakup

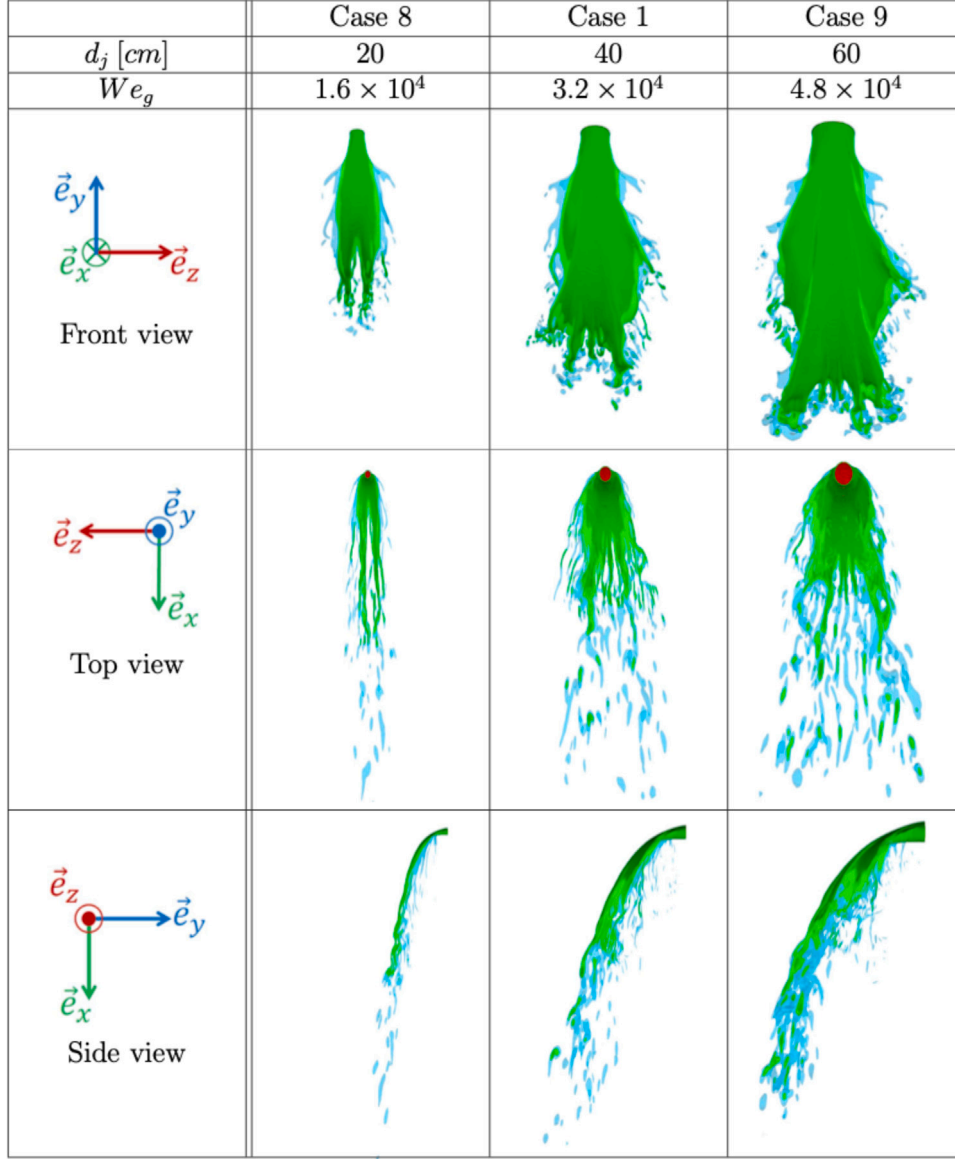


Fig. 19. Injector nozzle diameter  $d_j$  impact on the liquid column shape for a fixed momentum ratio  $q = 17.6$  at  $t = 4.5$  s for several views and for different liquid volume fractions  $\chi_j$  (blue :  $\chi = 0.1$  , green :  $\chi = 0.5$  and red :  $\chi_j = 0.9$  ). (For interpretation of the references to color in this figure legend, the reader is referred to the web version of this article.)

Coordinates :

$\vec{e}_x$  : Gaseous crossflow horizontal direction  
 $\vec{e}_y$  : Liquid jet injection (transverse) vertical direction

$\vec{e}_z$  : Spanwise horizontal direction

Liquid Jet in Gaseous Crossflow features :

$y$  : Liquid column penetration height in the transverse direction

$z$  : Liquid column expansion width in the spanwise direction

$x_{BU}$  : CBU streamwise length

$y_{BU}$  : CBU penetration height

Parameters :

$u$  : Velocity component in the  $x$  direction [  $\text{m s}^{-1}$  ]

$v$  : Velocity component in the  $y$  direction [  $\text{m s}^{-1}$  ]

$d_j$  : Liquid jet circular diameter at injector nozzle point [m]

$t$  : Time [s]

$\chi$  : VoF function

$\sigma$  : Surface tension [  $\text{N m}^{-1}$  ]

$\rho$  : Density [  $\text{kg m}^{-3}$  ]

$\mu$  : Dynamic molecular viscosity [  $\text{Pa s}$  ]

$I_j$  : Liquid jet turbulence intensity/level

$q = \frac{\rho_j v_j^2}{\rho_g u_g^2}$  : Liquid/air momentum flux ratio number

$We_g = \frac{\rho_g u_g^2 d_j}{\sigma}$  : Gas/aerodynamic Weber number

$We_j = \frac{\rho_j v_j^2 d_j}{\sigma}$  : Liquid jet Weber number

$Re_g = \frac{\rho_g u_g d_j}{\mu_g}$  : Gaseous crossflow Reynolds number

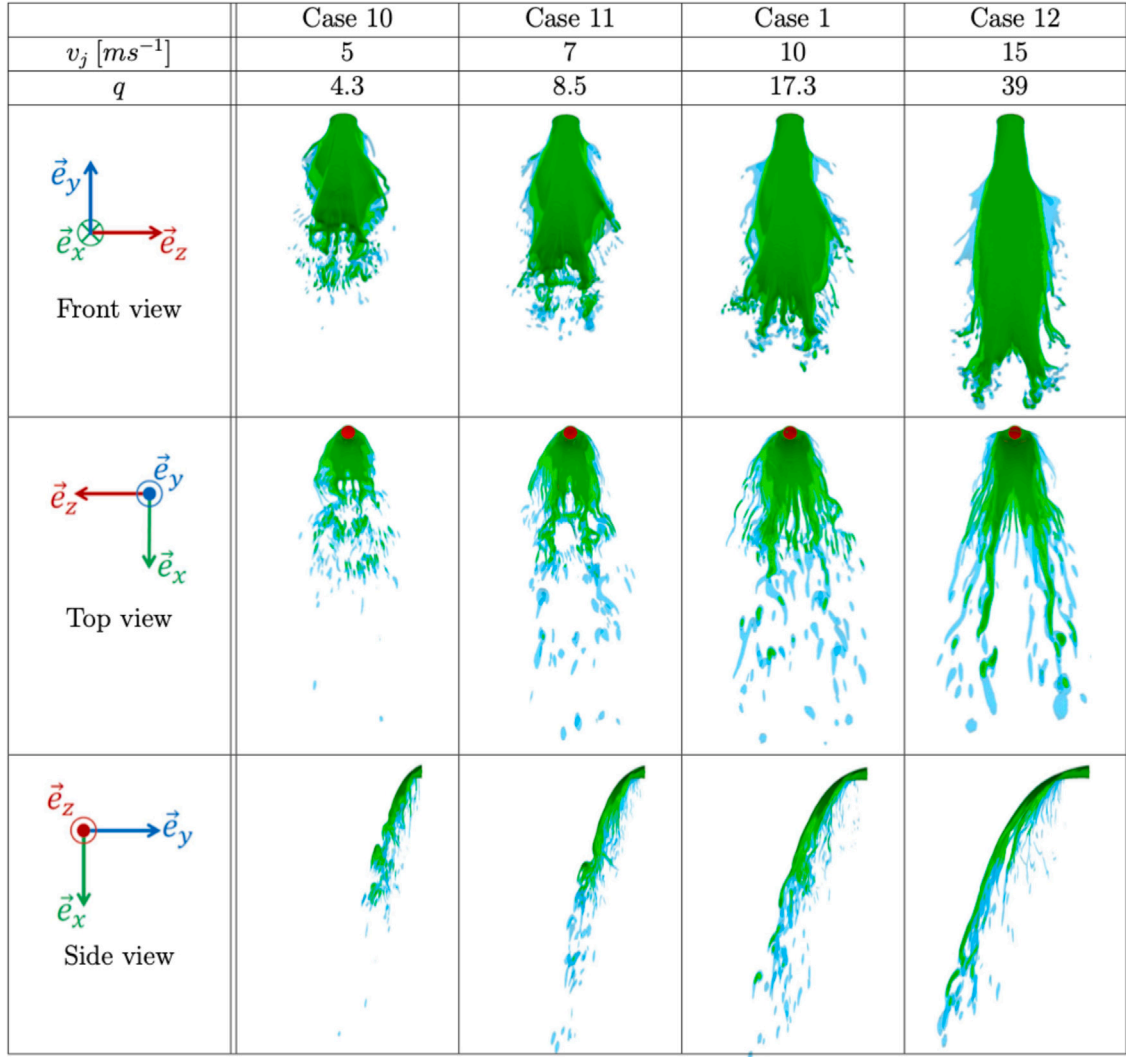


Fig. 20. Liquid jet velocity  $v_j$  impact on the liquid column shape for a fixed airflow Weber number  $We_g = 3.2 \times 10^4$  at  $t = 4.5$  s for several views and for different liquid volume fractions  $\chi$  (blue :  $\chi = 0.1$ , green :  $\chi = 0.5$  and red :  $\chi = 0.9$ ). (For interpretation of the references to color in this figure legend, the reader is referred to the web version of this article.)

$$Re_j = \frac{\rho_j v_j d_j}{\mu_j} : \text{Liquid jet Reynolds number}$$

$$Oh_j = \frac{\mu_j}{\sqrt{\sigma \rho_j d_j}} : \text{Liquid jet Ohnesorge number}$$

$$Bo = \frac{\rho_j g d_j^2}{\sigma} : \text{Bond number}$$

$$\rho^* = \frac{\rho_l}{\rho_g} : \text{Density ratio}$$

$$\mu^* = \frac{\mu_l}{\mu_g} : \text{Viscosity ratio}$$

#### Declaration of competing interest

The authors declare that they have no known competing financial interests or personal relationships that could have appeared to influence the work reported in this paper.

#### Data availability

Data will be made available on request.

#### Acknowledgments

The authors would like to thanks Frédéric Marsaly and Dan Reese for fruitful discussions. This project has benefited computation resources on the super computer CALMIP under the allowance 2020-P20015.

## Appendix

### A.1. Turbulence modeling test

See Fig. 18.

### A.2. Effect of the nozzle diameter

See Fig. 19.

### A.3. Effect of the liquid ejection velocity diameter

See Fig. 20.

### A.4. Effect of the air flow velocity

See Fig. 21.

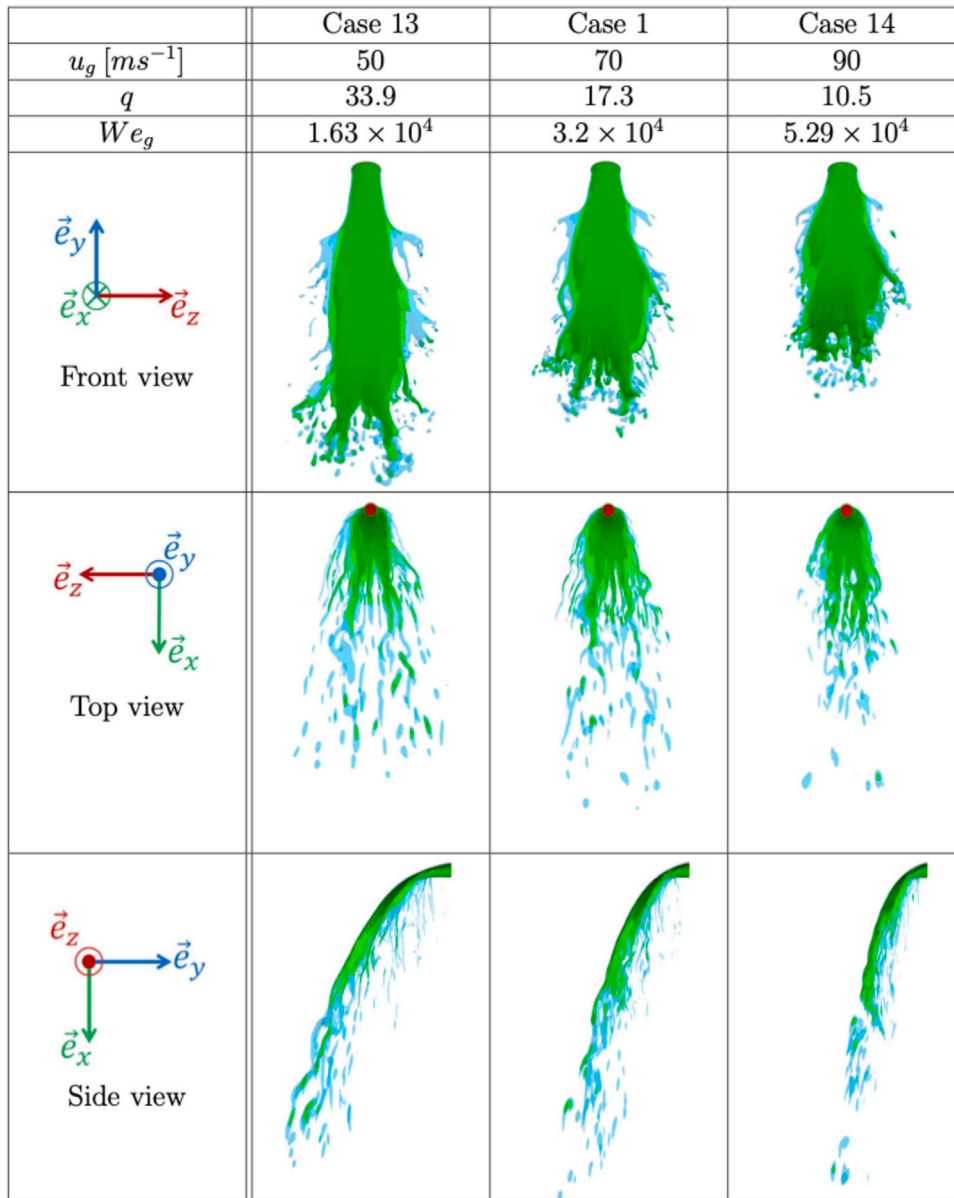


Fig. 21. Gaseous crossflow velocity  $u_g$  impact on the liquid column shape at  $t = 4.5$  s for several views and for different liquid volume fractions  $\chi$  (blue :  $\chi = 0.1$  , green :  $\chi = 0.5$  and red :  $\chi = 0.9$  ). (For interpretation of the references to color in this figure legend, the reader is referred to the web version of this article.)

## References

- Aalburg, C., van Leer, B., Faeth, G.M., Sallam, K.A., 2005. Properties of nonturbulent round liquid jets in uniform gaseous cross flows. *At. Spray.* 15, 271–294. <http://dx.doi.org/10.1615/AtomizSpr.v15.i3.20>.
- Ahn, K., Kim, J., Yoon, Y., 2006. Effects of orifice internal flow on transverse injection into subsonic crossflows: cavitation and hydraulic flip. *At. Spray.* 16, 15–34. <http://dx.doi.org/10.1615/AtomizSpr.v16.i1.20>.
- Amighi, A., Ashgriz, N., 2019a. Global droplet size in liquid jet in a high temperature and high-pressure crossflow. *AIAA J.* 57, 1–15.
- Amighi, A., Ashgriz, N., 2019b. Trajectory of a liquid jet in a high temperature and pressure gaseous cross flow. *J. Eng. Gas Turbines Power* 141, <http://dx.doi.org/10.1115/1.4042817>.
- Amighi, A., Eslamian, M., Ashgriz, N., 2009. Trajectory of a liquid jet in high pressure and high temperature subsonic air crossflow. In: 11th International Conference on Liquid Atomization and Spray Systems, Vail, Colorado, USA. paper No. 225.
- Becker, J., Hassa, C., 2002. Breakup and atomization of a kerosene jet in crossflow at elevated pressure. *At. Spray.* 12, 49–67. <http://dx.doi.org/10.1615/AtomizSpr.v12.i123.30>.
- Behzad, M., Ashgriz, N., Karney, B., 2016. Surface breakup of a non-turbulent liquid jet injected into a high pressure gaseous crossflow. *Int. J. Multiph. Flow.* 80, <http://dx.doi.org/10.1016/j.ijmultiphaseflow.2015.11.007>.
- Behzad, M., Ashgriz, N., Mashayek, A., 2015. Azimuthal shear instability of a liquid jet injected into a gaseous cross-flow. *J. Fluid Mech.* 767, 146–172. <http://dx.doi.org/10.1017/jfm.2015.36>.
- Behzad, M., Mashayek, A., Ashgriz, N., 2012. An analysis of the surface breakup mechanism of a liquid jet in cross-flow. In: 12th Triennial International Conference on Liquid Atomization and Spray Systems, ILASS - Europe, Heidelberg, Germany.
- Bellofiore, A., Cavaliere, A., Ragucci, R., 2007. Air density effect on the atomization of liquid jets in crossflow. *Combust. Sci. Technol.* 179, 319–342. <http://dx.doi.org/10.1080/00102200600809563>.
- Birouk, M., Iyogun, C.O., Popplewell, N., 2007. Role of viscosity on trajectory of liquid jets in a cross-airflow. *At. Spray.* 17, 267–287. <http://dx.doi.org/10.1615/AtomizSpr.v17.i3.30>.
- Brackbill, J., Kothe, D., Zemach, C., 1992. A continuum method for modeling surface tension. *J. Comput. Phys.* 100, 335–354.
- Broumand, M., Birouk, M., 2016. Liquid jet in a subsonic gaseous crossflow: Recent progress and remaining challenges. *Prog. Energy Combust. Sci.* 57, <http://dx.doi.org/10.1016/j.pecc.2016.08.003>.
- Broumand, M., Birouk, M., 2017. Effect of nozzle-exit conditions on the near-field characteristics of a transverse liquid jet in a subsonic uniform cross airflow. *Phys. Fluids* 29, 113303. <http://dx.doi.org/10.1063/1.4994978>.
- Broumand, M., Birouk, M., S. Vahid Mahmoodi, J., 2019. Liquid jet primary breakup in a turbulent cross-airflow at low weber number. *J. Fluid Mech.* 879, 775–792. <http://dx.doi.org/10.1017/jfm.2019.704>.



- Bury, Y., Morton, S., Charles, R., 2008. Experimental investigation of the flow field in the close wake of a simplified C-130 shape - A model approach of airflow influence on airdrop. In: 26th AIAA Applied Aerodynamics Conference, Honolulu, Hawaii, USA. pp. 1–21. <http://dx.doi.org/10.2514/6.2008-6415>.
- Cavaliere, A., Ragucci, R., Novello, C., 2003. Bending and break-up of a liquid jet in a high pressure airflow. *Exp. Therm Fluid Sci.* 27, 449–454. [http://dx.doi.org/10.1016/S0894-1777\(02\)00246-7](http://dx.doi.org/10.1016/S0894-1777(02)00246-7).
- Chelko, L., 1950. Penetration of liquid jets into a high-velocity air stream. In: Naca Research Memorandum. National Advisory Committee For Aeronautics, Washington, USA.
- Chen, T., Smith, C.R., Schommer, D.G., Nejad, A., 1993. Multi-zone behavior of transverse liquid jet in high-speed flow. In: 31st Aerospace Sciences Meeting and Exhibit, Reno, Nevada, USA, AIAA-93-0453. <http://dx.doi.org/10.2514/6.1993-453>.
- Cortelezzi, L., Karagozian, A.R., 2001. On the formation of the counter-rotating vortex pair in transverse jets. *J. Fluid Mech.* 446, 347–373. <http://dx.doi.org/10.1017/S0022112001005894>.
- Costa, M., Melo, M., Melo-de Sousa, J., Levy, Y., 2006. Spray characteristics of angled liquid injection into subsonic crossflows. *AIAA J.* 44, 646–653. <http://dx.doi.org/10.2514/1.10887>.
- Elshamy, O.M., Tambe, S.B., Cai, J., Jeng, S.M., 2007. Excited liquid jets in subsonic crossflow. In: 45th AIAA Aerospace Sciences Meeting and Exhibit, Reno, Nevada, USA, AIAA-2007-1340. pp. 1–10. <http://dx.doi.org/10.2514/6.2007-1340>.
- Eslamian, M., Amighi, A., Ashgriz, N., 2014. Atomization of liquid jet in high-pressure and high-temperature subsonic crossflow. *AIAA J.* 52, 1374–1385. <http://dx.doi.org/10.2514/1.J052548>.
- Farvardin, E., Johnson, M., Alaei, H., Martinez, A., Dolatabadi, A., 2013. Comparative study of biodiesel and diesel jets in gaseous crossflow. *J. Propuls. Power* 29, 1292–1302. <http://dx.doi.org/10.2514/1.B34743>.
- F.R., M., 1994. Two-equation eddy-viscosity turbulence models for engineering applications. *AIAA J.* 32 (8).
- Freitag, S., Hassa, C., 2008. Spray characteristics of a kerosene jet in cross flow of air at elevated pressure. In: 22nd European Conference on Liquid Atomization and Spray Systems, ILASS - Europe, Como Lake, Italy, paper ID ILASS08-12-1.
- Fuller, R.P., Wu, P.K., Kirkendall, K., Nejad, A.S., 1997. Effects of injection angle on the breakup processes of liquid jets in subsonic crossflows. In: 33rd Joint Propulsion Conference and Exhibit. <http://dx.doi.org/10.2514/6.1997-2966>.
- Gopala, Y., 2012. Breakup Characteristics of a Liquid Jet in a Subsonic Crossflow (Ph.D. thesis). Georgia Institute of Technology, Atlanta, Georgia, USA.
- Han, D., Orozco, V., Mungal, G., 2000. Cross-entrainment behavior of turbulent jets injected obliquely into a uniform crossflow. *AIAA J.* 38, 1643–1649. <http://dx.doi.org/10.2514/3.14591>.
- Haven, B.A., Kurosaka, M., 1997. Kidney and anti-kidney vortices in crossflow jets. *J. Fluid Mech.* 352, 27–64. <http://dx.doi.org/10.1017/S0022112097007271>.
- Herrmann, M., 2011. The influence of density ratio on the primary atomization of a turbulent liquid jet in crossflow. *Proc. Combust. Inst.* 33, 2079–2088. <http://dx.doi.org/10.1016/j.proci.2010.07.002>.
- Herrmann, M., Arienti, M., Soteriou, M., 2010. The impact of density ratio on the primary atomization of a turbulent liquid jet in crossflow. In: ASME Turbo Expo 2010. pp. 823–832. <http://dx.doi.org/10.1115/GT2010-23016>, aSME Turbo Expo 2010: Power for Land, Sea, and Air, GT 2010; Conference Date: 14-06-2010 Through 18-06-2010.
- Hirt, C., Nichols, B., 1981. Volume of fluid (vof) method for the dynamics of free boundaries. *J. Comput. Phys.* 39, 201–225. [http://dx.doi.org/10.1016/0021-9991\(81\)90145-5](http://dx.doi.org/10.1016/0021-9991(81)90145-5).
- Hussein, G.A., Jasuja, A.K., Fletcher, R.S., 1982. Penetration and break-up studies of discrete liquid jets in cross flowing airstreams. American society of mechanical engineers. In: 27th International Gas Turbine Conference and Exhibit, London, England. <http://dx.doi.org/10.1115/82-GT-25>.
- Inamura, T., 2000. Trajectory of a liquid jet traversing subsonic airstreams. *J. Propuls. Power* 16, 155–157. <http://dx.doi.org/10.2514/2.5547>.
- Inamura, T., Nagai, N., Hirai, T., Asano, H., 1991. Disintegration phenomena of metalized slurry fuel jets in high speed air stream. In: 5th International Conference on Liquid Atomization and Spray Systems, Gaithersburg, Maryland, USA. Vol. 7, pp. 839–846.
- Inamura, T., Nagai, N., Watanabe, T., Yatsuyanagi, N., 1993. Disintegration of liquid and slurry jets traversing subsonic airstreams. *Exp. Therm Fluid Sci.* 7, 166. [http://dx.doi.org/10.1016/0894-1777\(93\)90273-L](http://dx.doi.org/10.1016/0894-1777(93)90273-L).
- Iyogun, C.O., Birouk, M., Popplewell, N., 2006. Trajectory of water jet exposed to low subsonic cross-flow. *At. Spray.* 16, 963–980. <http://dx.doi.org/10.1615/AtomizSpr.v16.i8.70>.
- Kim, J.H., Ku, K.W., Youn, H.J., J.-G, H, Lee, C.W., Chung, K.Y., 2012. Effect of orifice configuration on the penetration height in crossflow. In: 12th Triennial International Conference on Liquid Atomization and Spray Systems, ICLASS - Europe, Heidelberg, Germany.
- Lee, K., Aalburg, C., Diez, F.J., Faeth, G.M., Sallam, K.A., 2007. Primary breakup of turbulent round liquid jets in uniform crossflows. *AIAA J.* 45, 1907–1916. <http://dx.doi.org/10.2514/1.19397>.
- Legendre, D., Becker, R., Almeras, E., Chassagne, A., 2014. Air tanker drop patterns. *Int. J. Wildland Fire* 23, 272–281. <http://dx.doi.org/10.1071/WF13029>.
- Li, X., Gao, H., Soteriou, M.C., 2017. Investigation of the impact of high liquid viscosity on jet atomization in crossflow via high-fidelity simulations. *Phys. Fluids* 29, 082103. <http://dx.doi.org/10.1063/1.4996178>.
- Li, X., Soteriou, M.C., 2016. High fidelity simulation and analysis of liquid jet atomization in a gaseous crossflow at intermediate weber numbers. *Phys. Fluids* 28, 082101. <http://dx.doi.org/10.1063/1.4959290>.
- Li, X., Soteriou, M.C., 2018. Detailed numerical simulation of liquid jet atomization in crossflow of increasing density. *Int. J. Multiph. Flow.* 104, <http://dx.doi.org/10.1016/j.ijmultiphaseflow.2018.02.016>.
- Lin, K.C., Kennedy, P.J., Jackson, T.A., 2002a. Penetration heights of liquid jets in high-speed crossflows. In: 40th Aerospace Sciences Meeting and Exhibit, Reno, Nevada, USA, AIAA-2002-0873.
- Lin, K.C., Kennedy, P.J., Jackson, T.A., 2002b. A review on penetration heights of transverse liquid jet in high-speed flows. In: 15th Annual Conference on Liquid Atomization and Spray Systems, ILASS - Americas, Madison, Wisconsin, USA. pp. 345–349. <http://dx.doi.org/10.2514/6.2002-873>.
- Liu, L., Fu, Q., Yang, L., 2021. Linear stability analysis of liquid jet exposed to subsonic crossflow with heat and mass transfer. *Phys. Fluids* 33, 034111. <http://dx.doi.org/10.13675/j.cnki.tjjs.2016.11.018>.
- Lubarsky, E., Shcherbik, D., Bibik, A., Gopala, Y., Zinn, B., 2012a. Fuel jet in cross flow - experimental study of spray characteristics. <http://dx.doi.org/10.5772/26045>.
- Lubarsky, E., Shcherbik, D., Bibik, O., Gopala, Y., Bennewitz, J.W., Zinn, B.T., 2012b. Experimental study of spray trajectories at elevated pressures and temperatures. In: 12th Triennial International Conference on Liquid Atomization and Spray Systems, ICLASS - Europe, Heidelberg, Germany.
- Madabhushi, R.K., Leong, M.Y., Arienti, M., Brown, C.T., McDonnell, V.G., 2006. On the breakup regime map of liquid jet in crossflow. In: ILASS - Americas, 19th Annual Conference on Liquid Atomization and Spray Systems, Toronto, Canada.
- Marsaly, F., 2016. Le boeing 747 supertanker d'evergreen. 09–27.fr Nouvelles des bords de pistes. <https://www.marsaly.fr/fred/le-boeing-747-supertanker-evergreen/>.
- Mashayek, A., Ashgriz, N., 2011. Atomization of a Liquid Jet in a Crossflow. Springer, pp. 657–683, (Chapter 29).
- Mashayek, A., Jafari, A., Ashgriz, N., 2008. Improved model for the penetration of liquid jets in subsonic crossflows. *AIAA J.* 46, 2674–2686. <http://dx.doi.org/10.2514/1.28254>.
- Mazallon, J., Dai, Z., Faeth, G.M., 1999. Primary breakup of nonturbulent round liquid jets in gas crossflows. *At. Spray.* 9, 291–312. <http://dx.doi.org/10.1615/AtomizSpr.v9.i3.40>.
- Mukundan, A.A., Tretola, G., Menard, T., Herrmann, M., Navarro-Martinez, S., Vogiatzaki, K., Motta, J.C.B., Berlemont, A., 2021. Dns and les of primary atomization of turbulent liquid jet injection into a gaseous crossflow environment. *Proc. Combust. Inst.* 38 (2), 3233–3241. <http://dx.doi.org/10.1016/j.proci.2020.08.004>.
- Muzafferija, S., Peric, M., 1998. Computation of free-surface flows using interface tracking and interface-capturing methods. In: Mahrenholtz, O., Markiewicz, M. (Eds.), *Nonlinear Water Wave Interaction*. Computational Mechanics Publications, Southampton, (Chap. 2).
- No, S.Y., 2015. A review on empirical correlations for jet/spray trajectory of liquid jet in uniform cross flow. *Int. J. Spray Combust. Dyn.* 7, 283–314. <http://dx.doi.org/10.1260/1756-8277.7.4.283>.
- Oda, T., Hiroyasu, H., Arai, M., Nishida, K., 1994. Characterization of liquid jet atomization across a high-speed airstream. *JSMIE Int. J. Ser. B: Fluids Therm. Eng.* 37, 937–944. <http://dx.doi.org/10.1299/jsmeb.37.937>.
- Osta, A.R., Sallam, K.A., 2010. Nozzle geometry effects on upwind surface properties of turbulent liquid jets in gaseous crossflow. *J. Propuls. Power* 26, 936–946. <http://dx.doi.org/10.2514/1.49737>.
- Pai, M., Bermejo-Moreno, I., Desjardins, O., Pitsch, H., 2010. Parametric study of primary breakup of turbulent liquid jets in crossflow: role of weber number. In: 48th AIAA Aerospace Sciences Meeting, Orlando, Florida, USA, AIAA-2010-212. <http://dx.doi.org/10.2514/6.2010-212>.
- Patankar, S., Spalding, D., 1972. A calculation procedure for heat, mass and momentum transfer in three-dimensional parabolic flows. *Int. J. Heat Mass Transfer* 15, 1787–1806. [http://dx.doi.org/10.1016/0017-9310\(72\)90054-3](http://dx.doi.org/10.1016/0017-9310(72)90054-3).
- Prakash, S.R., Jain, S.S., Lovett, J.A., Raghunandan, B.N., Ravikrishna, R.V., Tomar, G., 2019. Detailed numerical simulations of atomization of a liquid jet in a swirling gas crossflow. *At. Spray.* 29, <http://dx.doi.org/10.1615/AtomizSpr.2019031322>.
- Ragucci, R., Bellofiore, A., Cavaliere, A., 2007. Trajectory and momentum coherence breakdown of a liquid jet in high-density air cross-flow. *At. Spray.* 17, 47–70.
- Ryan, M.J., 2006. CFD prediction of the trajectory of a liquid jet in a non-uniform air crossflow. *Comput. Fluids* 35, 463–476. <http://dx.doi.org/10.1016/j.compfluid.2005.03.003>.
- Sallam, K.A., Aalburg, C., Faeth, G.M., Lin, K.C., Carter, C., Jackson, T., 2004. Breakup of aerated-liquid jets in supersonic crossflows. *At. Spray.* 16, 657–672. <http://dx.doi.org/10.1615/AtomizSpr.v16.i6.40>.
- Sallam, K.A., Ng, C.L., Sankararishnan, R., Aalburg, C., Lee, K., 2006. Breakup of turbulent and non-turbulent liquid jets in gaseous crossflows. In: 44th AIAA Aerospace Sciences Meeting and Exhibit, Reno, Nevada, USA, AIAA-2006-1517. <http://dx.doi.org/10.2514/6.2006-1517>.
- Scharfman, B.E., Bush, J.V.M., H.-A., T., 2013. Hydrodynamic instabilities in round liquid jets in gaseous crossflow. In: 25th Annual Conference on Liquid Atomization and Spray Systems, ILASS - Americas, Pittsburgh, Pennsylvania. pp. 405–412.

- Schetz, J., Kush, E., Joshi, P., 1980. Wave phenomena in liquid jet breakup in a supersonic crossflow. *AIAA J.* 18, 774–778. <http://dx.doi.org/10.2514/3.7687>.
- Schetz, J.A., Padhye, A., 1977. Penetration and breakup of liquids in subsonic airstreams. *AIAA J.* 15, 1385–1390. <http://dx.doi.org/10.2514/3.60805>.
- Shih, T.H., Yang, W.Z., A., S., Liou, W., Zhu, J., 1995. A new  $k-\epsilon$  eddy viscosity model for high reynolds number turbulent flow. *Comput. Fluids* 2 (3), 227–238, 4.
- Siemens, 2015. Star-ccm+ user guide. Available online: <https://fr.scribd.com/doc/193836790/Star-CCM-User-Guide>.
- Smith, S.H., Mungal, M.G., 1998. Mixing, structure and scaling of the jet in crossflow. *J. Fluid Mech.* 357, 83–122. <http://dx.doi.org/10.1017/S0022112097007891>.
- Song, J., Ahn, K., Kim, M.K., Yoon, Y., 2011. Effects of orifice internal flow on liquid jets in subsonic crossflows. *J. Propuls. Power* 27, 608–619. <http://dx.doi.org/10.2514/1.54203>.
- Stenzler, J.N., Lee, J.G., Santavicca, D.A., 2003. Penetration of liquid jets in a crossflow. In: 41st Aerospace Sciences meeting and Exhibit, Reno, Nevada, USA, AIAA-2003-1327.
- Stenzler, J.N., Lee, J.G., Santavicca, D.A., Lee, W., 2006. Penetration of liquid jets in a cross-flow. *At. Spray.* 16, 887–906. <http://dx.doi.org/10.1615/AtomizSpr.v16.i8.30>.
- Suter, A., 2002. Estimating Methods, Variability, and Sampling for Drop-Test Data. Tech. Rep. 0257-2826-MTDC, U.S. Department of Agriculture, Forest Service, Missoula Technology and Development Center, Missoula, MT, p. 30.
- Tambe, S.B., Elshamy, O.M., Jeng, S.M., 2007. Spray properties of liquid jets injected transversely into a shear layer. In: 43rd AIAA/ASME/SAE/ASEE Joint Propulsion Conference and Exhibit, Cincinnati, Ohio, USA, AIAA-2007-5695. <http://dx.doi.org/10.2514/6.2007-5695>.
- Tambe, S.B., Jeng, S.M., 2008. A study of liquid jets injected transversely into a swirling crossflow. In: 21st Annual Conference on Liquid Atomization and Spray Systems, ILASS - Americas, Orlando, Florida, USA.
- Thawley, S.M., Mondragon, U.M., Brown, C.T., McDonell, V.G., 2008. Evaluation of column breakpoint and trajectory for a plain liquid jet injected into a crossflow. In: 21st Annual Conference on Liquid Atomization and Spray Systems, ILASS - Americas, Orlando, Florida, USA. pp. 1–11.
- Thomas, R.H., Schetz, J.A., 1985. Distributions across the plume of transverse liquid and slurry jets in supersonic airflow. *AIAA J.* 23, 1892–1901. <http://dx.doi.org/10.2514/3.9193>.
- V., V., 1993. On the accuracy of limiters and convergence to steady state solutions. In: AIAA 93-0880, 31st Aerospace Sciences Meeting & Exhibit, Reno, NV, USA, Vol. 32, No. 8.
- Vich, G., Ledoux, M., 1997. Investigation of a liquid jet in a subsonic cross-flow. *Int. J. Fluid Mech. Res.* 24, 1–12. <http://dx.doi.org/10.1615/InterJFluidMechRes.v24.i1-3.10>.
- Wang, Q., Mondragon, U.M., Brown, C.T., McDonell, V.G., 2011. Characterization of trajectory, break point, and break point dynamics of a plain liquid jet in a crossflow. *At. Spray.* 21, 203–219. <http://dx.doi.org/10.1615/AtomizSpr.2011002848>.
- Wu, P.K., Fuller, R.P., Kirkendall, K.A., Nejad, A., 1997a. Breakup processes of liquid jets in subsonic crossflows. *J. Propuls. Power* 13, 64–73. <http://dx.doi.org/10.2514/2.5151>.
- Wu, P.K., Kirkendall, K.A., Fuller, R.P., Gruber, M., Nejad, A., 1997b. Spray trajectories of liquid fuel jets in subsonic crossflows. *Int. J. Fluid Mech. Res.* 24, 128–137. <http://dx.doi.org/10.1615/InterJFluidMechRes.v24.i1-3.130>.
- Wu, P.K., Miranda, R.F., Faeth, G.M., 1995. Effects of initial flow conditions on primary breakup of nonturbulent and turbulent liquid jets. *At. Spray.* 5, 175–196. <http://dx.doi.org/10.2514/6.1994-561>.
- Yates, C., 1971. Liquid injection into supersonic airstreams. In: AIAA/SAE 7th Propulsion Joint Special Conference, Salt Lake City, Utah, USA. pp. 71–724.
- Yoon, H.J., Hong, J., Lee, C., 2011. Correlations for penetration height of single and double liquid jets in cross flow under high-temperature conditions. *At. Spray.* 21, 673–686. <http://dx.doi.org/10.1615/AtomizSpr.2012004212>.
- Yu, D., Ali, M., Lee, J., 2006. Multiple tandem jets in crossflow. *J. Hydraul. Eng.* 132, 971–982. [http://dx.doi.org/10.1061/\(ASCE\)0733-9429\(2006\)132:9\(971\)](http://dx.doi.org/10.1061/(ASCE)0733-9429(2006)132:9(971)).
- Yuan, L., Street, R., 1998. Trajectory and entrainment of a round jet in crossflow. *Phys. Fluids* 10, 2323. <http://dx.doi.org/10.1063/1.869751>.
- Zheng, Y., Marshall, A.W., 2011. Characterization of the initial spray from low-Weber-number jets in crossflow. *At. Spray.* 21, 575–589. <http://dx.doi.org/10.1615/AtomizSpr.2011003714>.
- Zhu, Y., Sun, X., Sethi, V., Gauthier, P., Guo, S., Bai, R., Yan, D., 2021. Numerical investigation of the breakup mode and trajectory of liquid jet in a gaseous crossflow at elevated conditions. *Aeronaut. J.* 125, 1519–1541.